

Progress and Prospects of Emerging Potassium–Sulfur Batteries

Yao-Jie Lei, Hui-Ling Yang, Yaru Liang, Han-Wen Liu, Binwei Zhang, Liang Wang, Wei-Hong Lai,* Yun-Xiao Wang,* Hua-Kun Liu, and Shi-Xue Dou

The potassium–sulfur battery (K–S battery) as an innovative battery technology is a promising candidate for large-scale applications, due to its high energy density and the low cost of both K and S. The development of the K–S technology is, however, inhibited by its low reversible capacity and the safety issues related to the K metal anode. Here, the review starts by discussing the mechanism of the redox reactions for the K–S batteries and emphasizes the challenges for this battery system based on its current research status. Furthermore, the current improvement strategies for the K–S system in terms of the sulfur cathode, electrolyte, separator, and K metal anode are summarized. Finally, future perspectives on the development of the K–S system are proposed.

1. Introduction

Battery technologies have attracted great attention for grid support technology in many application fields. Among them,


Y.-J. Lei, H.-L. Yang, H.-W. Liu, L. Wang, W.-H. Lai, Y.-X. Wang, H.-K. Liu, S.-X. Dou
Institute for Superconducting and Electronic Materials
University of Wollongong
Wollongong, New South Wales 2500, Australia
E-mail: weihongl@uow.edu.au; yunxiao@uow.edu.au

Y. Liang
School of Materials Science and Engineering
Xiangtan University
Hunan 411105, China

B. Zhang
Center of Advanced Energy Technology and Electrochemistry
Institute of Advanced Interdisciplinary Studies
Chongqing University
Chongqing 400044, China

B. Zhang
College of Chemistry and Chemical Engineering
Chongqing University
Chongqing 400044, China

H.-K. Liu, S.-X. Dou
Institute of Energy Materials Science
University of Shanghai for Science and Technology
Shanghai 200093, China

 The ORCID identification number(s) for the author(s) of this article can be found under <https://doi.org/10.1002/aenm.202202523>.

© 2022 The Authors. Advanced Energy Materials published by Wiley-VCH GmbH. This is an open access article under the terms of the Creative Commons Attribution License, which permits use, distribution and reproduction in any medium, provided the original work is properly cited.

DOI: 10.1002/aenm.202202523

lithium-ion batteries (LIBs) have achieved great success.^[1] The severe situation of lithium resources, however, such as scarcity, drives the pursuit of a strategy for an alternative candidate, which is called “beyond LIBs.”^[2] Considering high energy, earth-abundance, pollution-efficiency, and cost-efficiency, the potassium–sulfur batteries (K–S batteries) have become a new favorite, deemed to be promising grid-scale battery systems.^[3] As an alternative to lithium, potassium possesses the following merits over lithium and sodium. First of all, potassium reserves have a very high natural abundance, which is

near to that of sodium in the Earth’s crust.^[4] The extraction of potassium from potassium carbonates (K_2CO_3) is cost-efficient as well.^[5] Moreover, compared with Li and sodium (Na), K is always endowed with unparalleled advantages in organic electrolytes.^[6] Potassium naturally exhibits a lower redox voltage (−0.09 V) when it is compared with those of Li and Na, which are 0 and 0.23 V, respectively. This lower redox voltage facilitates high voltage when potassium is used for a full battery. In addition, although the K atom possesses a larger radius (K/2.35 Å vs Li/1.55 Å, Na/1.90 Å), potassium shows a smaller Stokes’ radius (3.6 Å@K vs 4.8 Å@Li and 4.6 Å@Na) in carbonate-based solvents, due to the weaker Lewis acidity of potassium. K ions always exhibit high ion mobility, high ion conductivity, and a high ion transport number when carbonate solvents are used in electrolytes. Furthermore, with a low reduction potential ($E^0(K/K^+) = -2.93$ V versus the standard hydrogen redox potential), K could offer a high operating voltage and good gravimetric capacity.^[7] These advantages have made K the focus of increasing attentions. For instance, K is capable of insertion and extraction into/from graphite anode at low rates, where potassium graphite can be formed with a capacity of 278 mAh g^{−1}.^[8] Correlations and comparisons between Li, Na, and K are summarized in **Figure 1**. Sulfur, which benefits from the two-electron transfer redox between sulfur and sulfides (S^0/S^{2-}), exhibits a significantly high specific capacity of 1675 mAh g^{−1}, which has made sulfur a promising cathode materials.^[9]

To date, both Li–S and Na–S systems have undergone long study and are expected to be used in the fields of electric vehicles and grid-scale stationary energy storage, respectively.^[10] Compared with the values of the Li–S and Na–S battery systems in **Table 1**, the K–S battery features relatively lower gravimetric energy density, which is 1023 Wh kg^{−1} with potential of 2.1 V.^[11] Even so, this value is about two times higher than

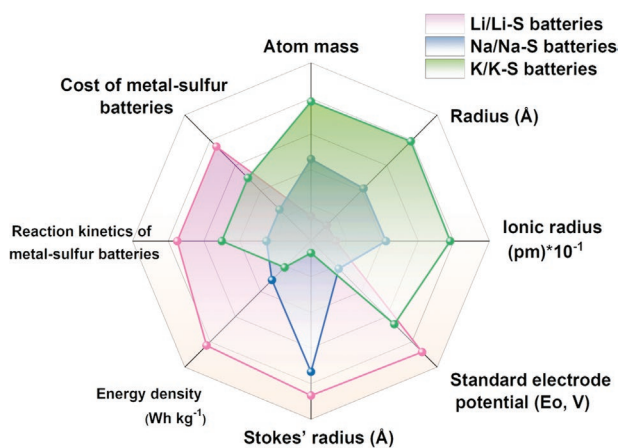


Figure 1. Comparison of physical properties for Li/Na/K and properties for Li-S/Na-S/K-S batteries.

that of commercial LIBs, thus serving as a promising battery technology for grid-scale stationary energy storage. Moreover, the high ionic conductivity of K ions, especially in ethylene carbonate electrolytes, endows K-S batteries with a satisfactory high rate capability. This is true, even though K metal seems to be more dangerous than Li and Na metal because K metal is more reactive and has a low melting temperature. Compared with the Li-S phase diagram and the Na-S phase diagram, the potassium polysulfide intermediates are all very stable at room temperature. Therefore, it is feasible to prepare some potassium intermediates as active materials instead of solid S. These polysulfide intermediates can be dissolved into an ether-based electrolyte, for example, tetraethylene glycol dimethyl ether (TEGDME), etc., to form a safe and stable polysulfide catholyte. When it comes to the anode side, hard carbon and graphite materials are superior and low-cost alternatives for K-metal-free K-S batteries, which deliver high performance for K-ion intercalation/deintercalation. This feature, to a large extent, addresses the safety risk of K-S batteries, leading to a very promising direction when compared with Li-S and Na-S batteries. Besides, the cost of cell production can be further reduced by replacing copper foils with cheap aluminum foils as anode current collectors (see Table 1 and Figure 1). As a result, the feasibility of novel K-S batteries for promising large-scale stationary applications is inspired by the encouraging merits of decent energy density and cost effectiveness.

Nevertheless, whatever kind of development of K-S batteries there is, such as, experimental research, understanding of the mechanism, and advanced characterization, this system is still in its early stages. In recent years, several efforts have been reported to improve the K-S system, relating

to nanoengineering optimization of S cathode materials,^[12] functionalized separators,^[13] novelty electrolytes,^[14] and anode strengthening.^[15] These are the basic components of the battery. In addition, one crucial question (different from Li and Na), which is the physical impact of potassium during charging and discharging processes, needs to be considered. Here, we collect the article publications based on the K-S battery. From the **Figure 2**, it can be witnessed that, since the first article related to potassium-sulfur battery was published in 2014,^[16] the K-S battery has continuously attracted research interest, as indicated by the increasing number of articles on this topic every year, but it is still less than for Li or Na batteries. Therefore, exploitation of the K-S system is a path well filled with hardship but remains surprising and full of potential.

2. Fundamental Properties of Sulfur Redox Reactions

Unlike Li-S and Na-S batteries, there are significant variations in regards of electrochemical kinetics and S reaction pathway at S cathode in K-S batteries, which prominently affect the electrochemical performance.^[22] Investigations into the mechanism have played a key role in improvement of the performance of the K-S system. As summarized in **Table 2**, the S redox reaction processes can be divided into two categories, which are solution-mediated reactions and solid-solid reactions, respectively. The reaction pathways are mainly determined by the types of electrolyte solvents. For the typical ether-based electrolyte, the long-chain potassium polysulfide intermediates K_2S_x ($5 \leq x \leq 8$) can be dissolved into solvents as a liquid phase and then converted into insoluble short-chain K_2S_y ($3 \leq y \leq 1$) leading to a typical solid-liquid-solid pathway, denoted as a solution-mediated reaction. In contrast, the solid-solid reaction tends to be present in carbonate-based electrolytes, in which the S redox reaction processes are isolated from the electrolyte with all reaction intermediates and final products in the solid phase.

2.1. Solution-Mediated Pathway

2.1.1. Solid Sulfur Molecules (S_8)

Figure 3 presents typical and idealized discharge and charge curves of cathodes in metal-sulfur batteries. All the curves relate to cathodic S with no carbon host in normal ether electrolytes. Similar to Li-S and Na-S batteries, the S in the cathode would experience a reversible redox reaction, while the K metal would be subjected to plating and stripping processes during charge

Table 1. Comparisons of properties for Li-S, Na-S, and K-S batteries.

Battery types	Working temperatures	Energy density [Wh kg ⁻¹]	Reaction kinetics	Cost	Applications
Li-S batteries	Room temperature (RT)	2571	Fast	High	Long-range electrical vehicles
Na-S batteries	RT to 300 °C	1273	Slow	Low	Grid-scale stationary energy storage
K-S batteries	RT to 150 °C	1023	Medium	Medium	Grid-scale stationary energy storage

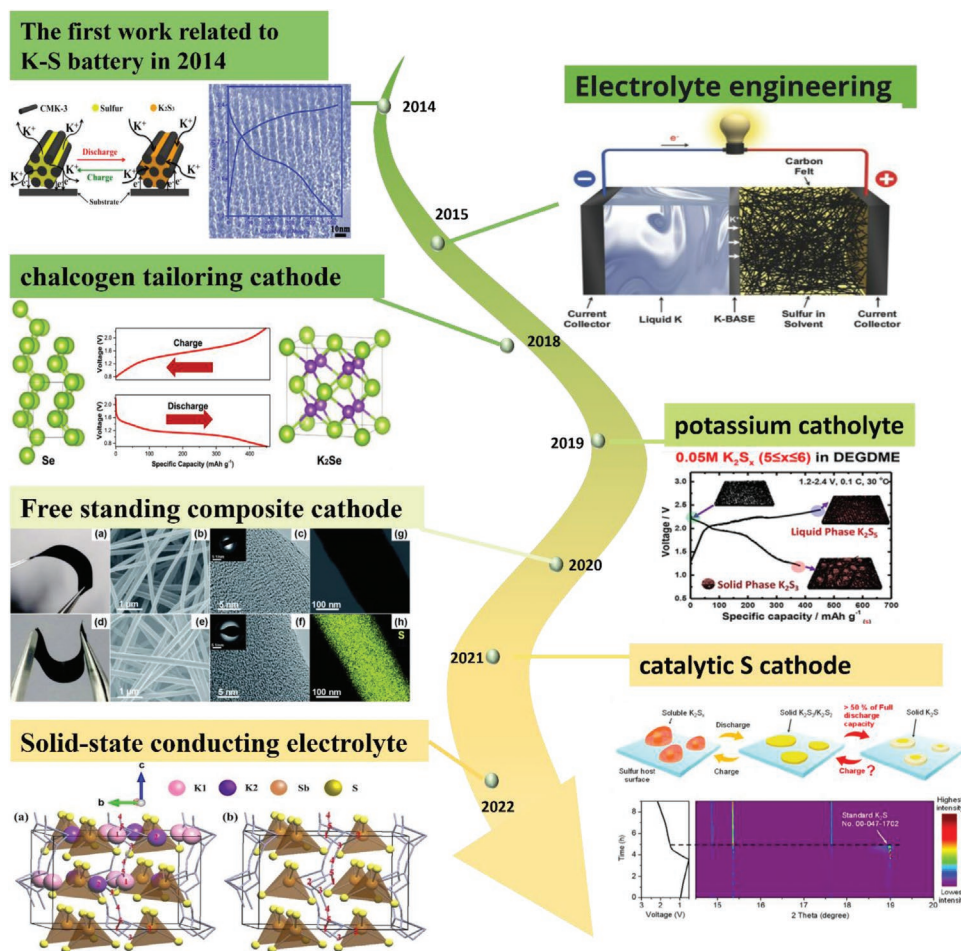
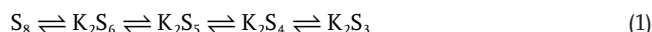


Figure 2. A brief chronicle of the developments for K–S batteries. The first work related to K–S battery in 2014: Reproduced with permission.^[16] Copyright 2014, American Chemical Society. Electrolyte engineering: Reproduced with permission.^[17] Copyright 2015, Wiley-VCH. Chalcogen tailoring cathode: Reproduced with permission.^[18] Copyright 2017, Elsevier. Potassium catholyte: Reproduced with permission.^[14] Copyright 2018, American Chemical Society. Free standing composite cathode: Reproduced with permission.^[19] Copyright 2020, The Royal Society of Chemistry. Catalytic S cathode: Reproduced with permission.^[20] Copyright 2021, American Chemical Society. Solid-state conducting electrolyte: Reproduced with permission.^[21] Copyright 2022, Wiley-VCH.

and discharge.^[26] In the meantime, the K ions migrate to/from the electrolyte while the electrons go through the external circuit. Sulfur exists in many allotropes, which can be divided into the ring and chain allotropes.^[30] Usually, the long-sulfur (8) is always in the ring form, while short-sulfur (2-4) is always chain. If the S undergoes an intact discharge, which is a two-electron charge-transfer process, it can deliver the theoretical capacity of 1675 mAh g⁻¹, although that is the ideal condition. The K–S battery releases a relatively lower energy density, due the lower discharge voltage (1.88 V) and larger size of potassium (compared with Li–S and Na–S). S₈ is first reduced to K₂S_x polysulfides, which are further decreased to K₂S_y polysulfides. The K₂S_y K-polysulfides cannot dissolve in the ether solvents, causing the formation of K₂S₃/K₂S₂/K₂S, solid species. These thus-formed species would easily deposit on the surface of the cathode and not be involved in reactions any more in the following cycles.^[24,31] Wang et al. fabricated mesoporous carbon (CMK-3) infiltrated with sulfur as their cathode material.^[32] With the help of ultraviolet-visible absorption spectroscopy (UV-vis) and X-ray diffraction (XRD), they acquired reversible immediate phase conversion as follows:



According to recent research on the K–S battery, K₂S₃ has been proved to be the final discharge product on the cathode by transmission electron microscopy (TEM), X-ray photoelectron spectroscopy (XPS), Raman spectroscopy, XRD, etc. In discharge and charge processes, there is no trace of K₂S to be found during a galvanostatic cycling test with the voltage window between 1.2 and 3 V, illustrating that there is no K₂S formation. This phenomenon is caused by the sluggish reduction kinetics, leading to an incomplete reduction reaction from K₂S₃ to K₂S.^[33] In addition, K₂S₃ is endowed with higher thermodynamic stability, with a Gibbs formation energy of –528 kJ mol⁻¹, while that of K₂S is –410 kJ mol⁻¹.^[34] Furthermore, unlike the unstable or inseparable polysulfides in the Li–S system, the polysulfide intermediates in K–S system occur in a series of stable phases, which has made it convenient for researchers to discover the mechanism by using pure-phase K-polysulfides. After the current collector was coated with K₂S₂ and K₂S₃, these two intermediates would be further reduced to K₂S, demonstrating that a solid-state conversion had occurred.

Table 2. The two pathways of S redox reactions in K–S batteries.

Category	Sulfur cathode	Sulfur structure	Electrolyte	Sulfur loading ratio	Cut-off voltage	Final discharge product	Sulfur redox reaction
Solution-mediated pathway	PANI coated CMK-3/S ^[16]	S ₈	1 m KClO ₄ in TEGDME	28%	1.2–2.4 V	K ₂ S ₃	Discharge: 3S + 2K ⁺ + 2e ⁻ → K ₂ S ₃ Charge: K ₂ S ₃ ·2e ⁻ → 3S + 2K ⁺ Overall: 3S + 2K ⇌ K ₂ S ₃
	K ₂ S ₅ catholyte ^[14]	K ₂ S ₅	0.5 m KTFSI in DEGDM	–	1.2–2.4 V	K ₂ S ₃	Discharge: K ₂ S _x (5 ≤ x ≤ 6) → K ₂ S ₃ Charge: K ₂ S ₃ → K ₂ S ₅ Overall: K ₂ S _x ⇌ K ₂ S ₃
	Catholyte: Sulfur + K ₂ S _x ^[17]	K ₂ S ₅	1.5 m KTFSI in DME	–	1.2–3.0 V	K ₂ S ₃	Discharge: K ₂ S ₅ → K ₂ S ₄ + K ₂ S ₃ → K ₂ S ₃ + K ₂ S ₂ Charge: K ₂ S ₂ → K ₂ S ₃ + K ₂ S ₄ → K ₂ S ₅ Overall: K ₂ S ₅ ⇌ K ₂ S ₂
Solid–solid pathway	PCNF/S ^[23]	S _n (n ≤ 3)	KPF ₆ in EC/DEC	25%	0.5–3.0 V	K ₂ S	S _n ⇌ K ₂ S
	SPAN ^[24]	–C–S _x –C–	0.8 m KPF ₆ in EC/DMC	45.5%	0.5–3.0 V	K ₂ S ₃	S ⇌ K ₂ S
	Small-molecule sulfur ^[25]	S _n (n ≤ 3)	KPF ₆ in EC/DEC	20%	0.5–3.0 V	K ₂ S	S ⇌ K ₂ S
	S@SA-NC ^[20]	S ₈	(KPF ₆) in EC/DEC	56.8%	0.5–3.0 V	K ₂ S	Discharge: S ₈ → K ₂ S Charge: K ₂ S → K ₂ S _n
	S/CNF ^[26]	S ₈	1 m KCF ₃ SO ₃ in TEGDME	50%	1.0–2.8 V	K ₂ S	S ₈ ⇌ K ₂ S ₆ ⇌ K ₂ S ₄ ⇌ K ₂ S ₂ ⇌ K ₂ S
S–N–Co ₃ –C polyhedron ^[27]	S ₈	0.8 m KPF ₆ in EC/DEC	62.4	0.5–2.8 V	K ₂ S ₃	3S + 2K ⇌ K ₂ S ₃	

Afterward, the discharge products (K₂S₂, K₂S₃, and K₂S) also were charged immediately. After isolation of the charge products, both K₂S₂ and K₂S₃ could be charged via solution-mediated charging. K₂S, however, became the dead species that could not be charged.^[33]

2.1.2. Polysulfide Catholyte

Instead of traditional S solid, Hwang et al. used K₂S_x as catholyte and designed a novel K–S cell, which was K|K₂S_x catholyte|CNT, where CNT is carbon nanotube (CNT), to

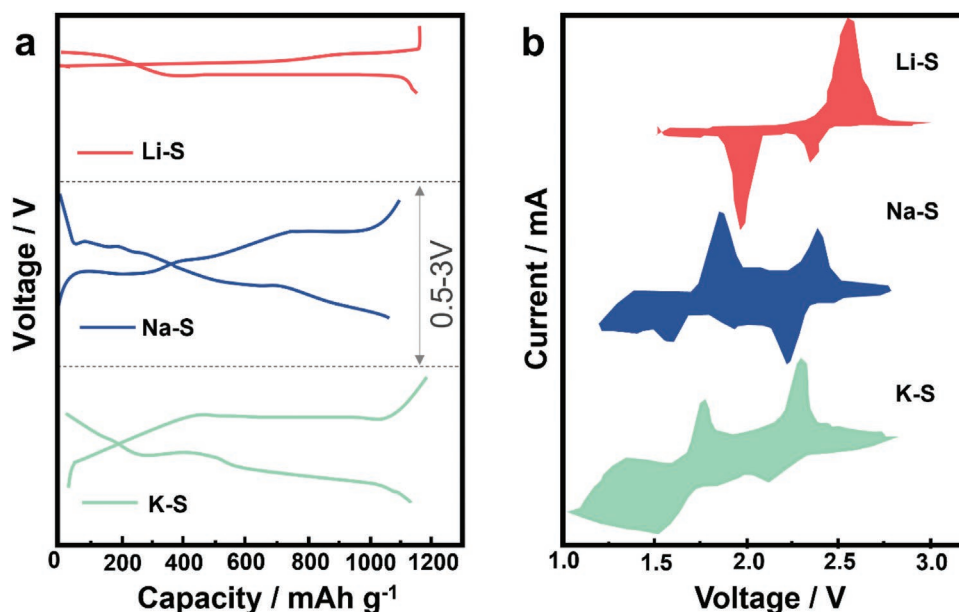
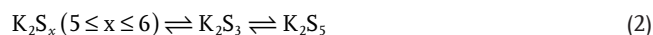


Figure 3. Representative metal-sulfur battery discharge–charge curves. a) Discharge–charge curves of Li–S battery, Na–S battery, and K–S battery. b) Cyclic voltammetry (CV) curves of Li–S battery, Na–S battery, and K–S battery. Curves of Li–S battery: Reproduced with permission.^[28] Copyright 2013, American Chemical Society. Curves of Na–S battery: Reproduced with permission.^[29] Copyright 2018, Wiley-VCH. Curves of K–S battery: Reproduced with permission.^[26] Copyright 2018, Elsevier.

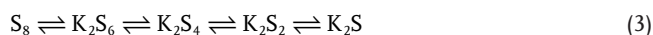
investigate the electrochemical mechanism.^[14] From a combination of ex situ Raman spectra and XRD patterns, they demonstrated that K_2S_3 is the final product and that it can be mutually converted to and from K_2S_5 . Hence, this reversible reaction can be summed up as:



For the solution-mediated pathway, no matter what the S structure is, such as S_8 , or K_2S_x liquid polysulfides, the reversible reactions are based on the conversion between liquid polysulfides and solid K_2S_3 . The conversion processes of K_2S_3 to K_2S in ether-based electrolytes tend to be terminated due to the sluggish kinetics of the solid phase reactions. The introduction of catalytic sites into the S cathode can be a rational strategy to accelerate the kinetics and reversibility of the solid conversion.

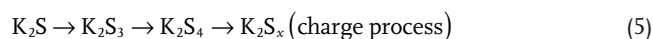
2.2. Solid–Solid Pathway

Researchers discovered that a discharge plateau obviously exists when the voltage is held at 1.6–1.2 V, which is very similar to the cases of Li–S and Na–S systems.^[10a,35] In order to verify this assumption, Yu found that K_2S exists from X-ray XPS, suggesting reformation of S after charging.^[26] This consequence can be indicated as:



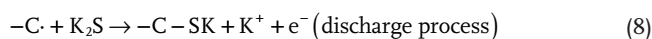
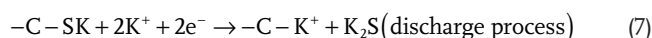
2.2.1. Atomic Catalysts for S_8

The liquid-mediated pathway means that S cathode exhibit incomplete redox reaction, the final product of which is K_2S_3 . The theoretical capacity from S to K_2S_3 only delivers 33% of the whole cathodic capacity of the complete S redox reaction. To maximize the complete S capacity of the cathode, it is important to facilitate K_2S formation during the discharge process and oxidation during the charge process. To achieve the complete reversible reaction on S cathode, Qiao's group introduced cobalt (Co) single atomic catalysts with more powerful catalytic functions (Figure 4a).^[20] The Co single-atoms act as efficient catalysts that can promote S reduction conversion on the cathode. Due to dynamics of the Co–S interaction, the K–S bonds can be dissociated during the charging process, which facilitates the oxidation of K_2S . Thus, the Co atomic catalysts are favorable for the solid–solid reaction, which allows K–S batteries achieve the excellent electrochemical performance. According to results of in situ XRD, K_2S is the final discharge product while K_2S can also be oxidized to high-ordered polysulfides during the charging. Thus, the conversion reaction of S cathode can be expressed as:



2.2.2. Covalent S

In view of the above research studies, many workers concluded that the reduction of K_2S_3 to K_2S takes place because of the disproportionation and comproportionation reactions between the polysulfides instead of direct formation.^[24] Xiong et al., relying on theoretical density functional theory calculations further achieved insights into the basic reaction mechanisms of the K–S system, and they indicated that K_2S_2 has a tendency to form K_2S_3 and K_2S , which is due to the higher formation energy of K_2S_2 compared with K_2S_3 and K_2S .^[25] This conclusion was verified by Sun's group (Figure 4b). They constructed a sulfurized PAN (SPAN) electrode with polyacrylic acid (PAA) binder and analyzed final discharge product by using XPS measurements, which showed that K_2S , K_2S_2 and K_2S_3 exist simultaneously on the electrode after discharging.^[24] It is commonly known that the theoretical capacity of K_2S_3 – K_2S account for 67% of whole S capacity (1675 mAh g^{-1}). Actually, the covalent S in the SPAN electrode undergoes the complete redox reaction, which makes the final discharge product K_2S . This reaction maximizes the full discharge S capacity during the discharging process, which makes SPAN-S exhibit a very high capacity. Hence, the reactions of the SPAN electrode in the K–S batteries could be expressed as:



2.2.3. Small Molecular S

The S conversion reaction process for small molecular forms of S, such as S_2 , S_3 , is different from that of the S_8 cathode.^[25] During the discharge process, the small molecular S is reduced to solid-state K_2S_y polysulfide intermediates and then to K_2S by a solid–solid reaction pathway. During the charge process, insoluble K_2S is transformed to small molecular S (S_2 , S_3) (Figure 4c). No soluble K_2S_x polysulfide intermediates form in this process due to the space confinement by micropores. Therefore, this mechanism could be indicated as:



Due to the sluggish kinetics of solid–solid processes, the success of K–S batteries in carbonate-based electrolyte is determined by the high activity of the S cathode. This high activity can be achieved via constructing covalent S, confining small molecule S or incorporating catalysts.

To conclude, from the above discussion and analysis, K_2S , K_2S_2 , and K_2S_3 have all been successfully characterized as final products during discharging. In regards to stability, they could be arranged as $K_2S_3 \geq K_2S \geq K_2S_2$.^[36] Considering, however, the disproportionation and comproportionation reactions between these polysulfide intermediates, K_2S_3 would be further reduced

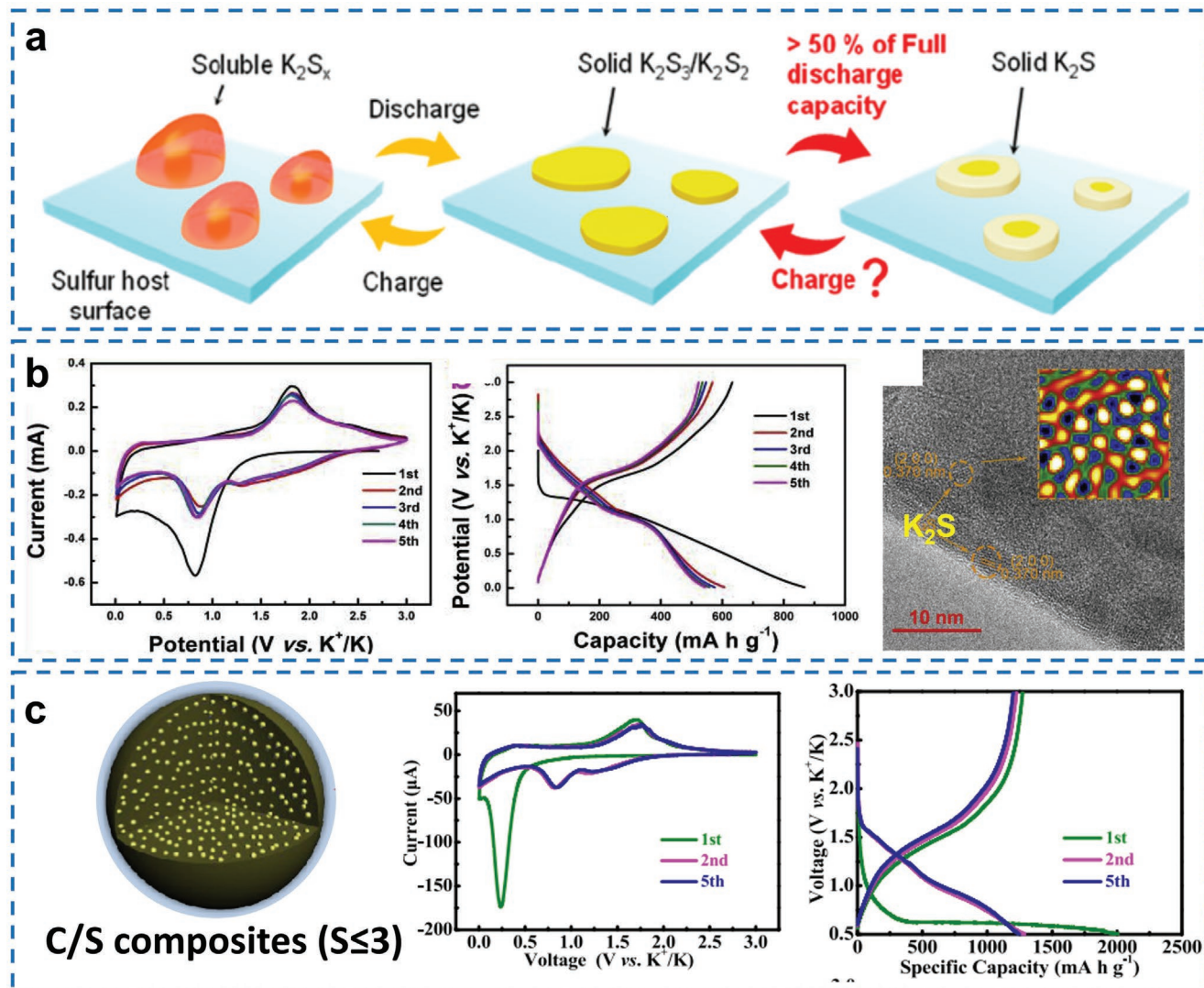


Figure 4. a) Schematic illustrations of discharge and charge in K–S batteries with atomic catalysts for S_8 . Reproduced with permission.^[20] Copyright 2021, American Chemical Society. b) CV curves, charge–discharge profiles and TEM images of the final discharge product in K–S batteries for covalent S. Reproduced with permission.^[24] Copyright 2018, Elsevier. c) Schematic illustration of S states in the porous carbon matrix, CV curves, and charge–discharge profiles in K–S batteries for small molecular S. Reproduced with permission.^[25] Copyright 2019, American Chemical Society.

to K_2S_2 and K_2S . At the same time, K_2S_2 also undergoes a difficult reduction reaction (solid state conversion) to form K_2S .^[17] Therefore, we can reach the conclusion that K_2S_3 , K_2S_2 , and K_2S coexist as final products during the charging process and determine what kind of product is dependent on the different materials in different systems.

Current characterization techniques are insufficient to accurately determine the final product. More innovation and advanced techniques need to be involved to analyse the K–S system, for instance, synchrotron techniques (X-ray absorption spectroscopy (XAS), in situ XAS, in situ XRD, in situ far-infrared spectroscopy), in situ TEM, nuclear magnetic resonance (NMR), and time-of-flight-secondary ion mass spectrometry (TOF-SIMS), which are all very important for characterizing the ambiguous K–S battery mechanism. For example, the sluggish kinetics often results in a core-shell structure of K-polysulfides during the potassiation process. Synchrotron techniques could

establish how decreasing the K content (from the exterior toward the interior centre) affects K-polysulfides and creates core-shell structures. In addition, synchrotron techniques can not only help us to clarify the nature of the final discharging products, but also realize the whole dynamic evolution process of S (from S_8 to final products) at a given voltage.

3. Challenges of the K–S system

Compared with the Li–S battery and the Na–S battery, the development of the K–S battery is in its early stages. Therefore, many challenges still need to be addressed in the K–S battery system. With full realization of the challenges for the K–S battery, we can design targeted K–S batteries with excellent performance. Before achieving high energy density and cycling stability in the K–S system, however, its interfacial chemistry

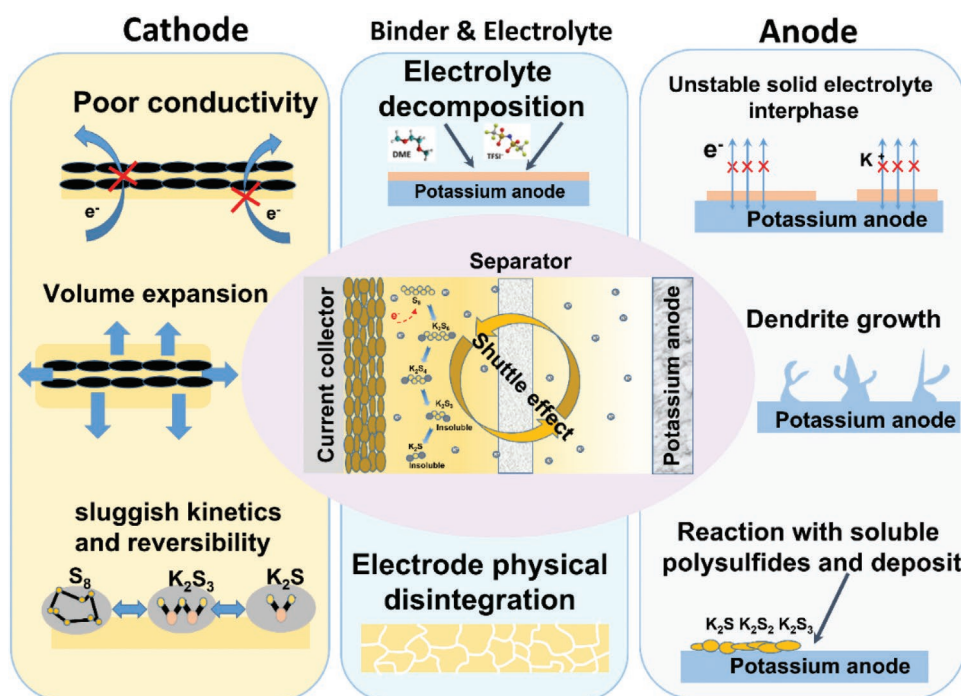


Figure 5. Main challenges of K–S batteries.

and ion diffusion, as well as the relationships among them need to be further understood to address the main challenges for the K–S system (Figure 5).

3.1. Polysulfide Shuttle

Similar to its Li–S and Na–S counterparts, the dissolution of polysulfides also exists in K–S batteries. In ether electrolyte, the high dissolution of K_2S_x polysulfides would cause soluble polysulfides to inevitably migrate from the cathode side to the anode side. Then these K_2S_x polysulfides would react with potassium metal on the anode to form insoluble K_2S_y polysulfides and be further deposited on the surface of the anode. This phenomenon is the so-called “shuttle effect,” which is the main culprit for low efficiency and rapid decay of cycling capacity.^[37] In the meantime, dissolved polysulfide could react with fresh potassium metal in the anode and further form low-dissolution K_2S_y polysulfides (K_2S_2 , K_2S), which are in the solid state. The K_2S_y polysulfides will be deposited on the surface of the potassium anode, which is the main issue causing active materials loss. In addition, due to the concentration gradient, the polysulfides deposited on the surface of the anode subsequently consume the charge currents, which make the K–S batteries unable to complete the whole charge process, leading to low coulombic efficiency. Moreover, after the polysulfides continuously settle on the anode side and react with the potassium anode, the discharge capacities and voltage plateaus will fall. In addition, such insoluble K_2S_y polysulfides will generate a rough surface on the anode side, causing the acceleration of potassium dendrite growth. Last but not least, the high activity of soluble polysulfides would decrease the selection of liquid

organic solvents. Consequently, the nucleophilic and electrophilic solvents, including ester, aldehyde, ketone, etc., will be excluded.

3.2. Thermodynamic Prohibition Issue for K_2S_3

Currently, the electrochemical reaction mechanism of K–S batteries is still not well understood. Unlike Li–S and Na–S batteries, the K_2S_y polysulfides in the K–S chemical diagram, including K_2S , K_2S_2 , K_2S_3 , and K_2S_4 , are all in the solid state in ether-based electrolytes. Regardless of whether the solid potassium polysulfides are further reduced or oxidized, solid potassium polysulfides possess inferior kinetics. For instance, the K_2S is hardly oxidized during the charge process. At present, many works report that K_2S_3 is the final product in K–S batteries rather than K_2S .^[16] Ye et al. demonstrated, however, that K_2S is the final product, which was verified by synchrotron-based XRD.^[16] In addition, the products corresponding to different voltage windows are unclear as well. Therefore, more research works on the cathode should be designed to address these challenges.

3.3. Electrolytes

3.3.1. Severe Side Reactions and Electrolyte Consumption for Liquid Electrolyte

Side reactions between polysulfides and the electrolyte occur at a typical lower cut-off voltage than for the other alkali metals, which cause low initial coulombic efficiency in the first cycle

and even cell failure. Severe side reactions could rapidly consume and exhaust the electrolyte. It is notable that due to substitution or nucleophilic addition reactions, long-chain polysulfides would easily react with the electrolyte (carbonate-based solvents), causing a direct loss of sulfur.^[20] In addition, the low electrochemical potential of K can easily cause a solvent reduction on the electrode surface, leading to formation of solid–electrolyte interphase (SEI) film on the K anode. This SEI is always unstable and roughens the anode surface, which can cause consecutive side reactions with the electrolyte during the K–S battery operation, leading to potassium consumption and decreased electrolyte effectiveness. As a result, the bad influence of the K–S battery would cause inferior cycling and low coulombic efficiency.

3.3.2. Low Ionic Conductivity and High Interfacial Resistance for Solid-State Electrolytes

Although performing the solid-state electrolytes can entirely suppress the shuttling effect, the high interfacial resistance, and low ionic conductivity in room temperature would cause inferior rate performance and cycling stability. First, the connection between solid electrolyte and electrode material is in solid state, so the effective contact between electrode and electrolyte is weak, and the ion transport kinetics in solid material is low. It will cause the interface impedance is too large. In term of ionic conductivity, it is the key factor to determine the internal resistance and multiplier performance of a battery. The electrolyte should be insulated from electrons as much as possible while improving ionic conductivity, which voids the self-discharging process. Besides, the mechanical strength, chemical, as well as, thermal stability needs to be further improved. The mechanical strength of electrolytes is a significant factor to be considered for the production of batteries. The solid-state electrolyte should be elastic instead of brittle during the processing and assembly. Meanwhile, the solid-state electrolytes could not react with other components of the battery, including cathode, anode, collector, separator, additive, and packaging materials, etc. The thermal stability can ensure the safety of the battery in the case of short circuit, overcharge, and heat, etc.

3.4. Volume Fluctuation and Physical Disintegration of the Electrode during Potassiation/Depotassiation

Due to the large size of potassium ions, it could damage the integrity of the electrodes and result in pulverization. This phenomenon may raise further concerns about the side reactions on the SEI layer on the cathode. In regard to the anode, side reactions would lead to dendrite growth and even the fracturing of the SEI during plating and stripping. The SEI will also continuously form, which will consume a large amount of electrolyte and enhance the polarization of the electrode. As a result, capacity will fade quickly. Furthermore, the cathode would easily suffer from volume change during potassiation and de-potassiation processes because of the large radius of the potassium ion.^[38] This is the key issue that may cause the physical disintegration of electrode materials during cycling. When

K_2S_8 is oxidized to K_2S , the volume will be greatly expanded by 296%, whereas its counterpart (Li) is enlarged by 80%. The expansion related to potassium poses a huge challenge for the design of cathode materials. Many carbon architectures for Li–S and Na–S may be inadequate for the K–S system, because they insufficiently support severe volume change.

3.5. Dendrite Growth

Troubles at the potassium metal anode are the key issue causing poor coulombic efficiency (CE). The specific capacity of potassium metal is 687 mAh g^{-1} , which is two times that for lithium insertion into graphite.^[39] This makes it likely that unstable potassium will be obtained during plating and stripping processes. Unstable plating and stripping would result in fluctuations in the metal front surface and the SEI, which continuously consumes the metal anode and electrolyte. Hence, the optimized S-based cathode will be indirectly broken. Also, an unstable SEI film can cause dendrite formation, which is usually the source of cell shorting. The dendrite growth originates from localized electrical field concentrations and ion-diffusion limitations. Unlike the dendrite growth of Li and Na metal, the dendrite growth of K is more complicated. The specific manifestation is dendrites with mossy or forest-like architecture rather than a needle-like structure, which results from the faster diffusion of K ions.^[40] Therefore, in the K–S system, the potassium metal anode needs to be optimized to achieve excellent performance.

4. Classification of Improvements Strategies for the K–S System

Now, the performance of a metal-sulfur system is generally evaluated in typical coin-type cells, which consist of potassium metal as anode, sulfur-loaded composite as cathode, a separator, and an electrolyte. All the works to improve the performance of metal-sulfur systems relate to these four aspects. Furthermore, the larger size of the potassium ion can shock the host material and then make the electrode physically disintegrate, which can be regarded as the fifth aspect. In this review, we first discuss the electrochemical mechanism of K–S system batteries and systematically collate current developments based on these five aspects, as schematically illustrated in **Figure 6**, including various approaches to the cathode, anode, electrode immobilization, and functionalized separators, as well as, electrolyte optimization.

4.1. Strategies for the Sulfur Cathode

Because the above challenges threaten the practical reliability of the K–S system, it is necessary to address these intrinsic issues. In the case of the sulfur cathode, the designed strategies should be based on sulfur conversion chemistry, which is the main “source” of low sulfur utilization and poor cycling performance. In this respect, carbonaceous materials have attracted increasing attention for use as sulfur cathode materials.^[41] There are several advantages of using carbon-based materials as cathode materials for the K–S system: 1) The carbon matrix

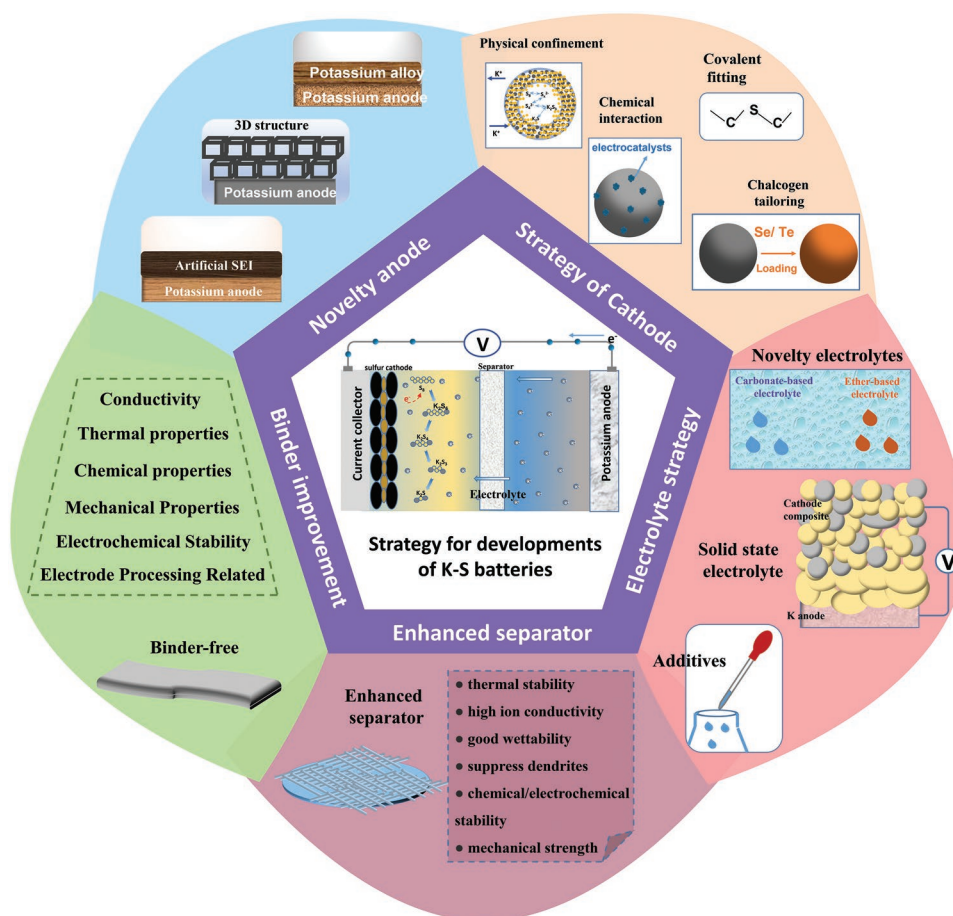


Figure 6. Schematic diagram of developments and study trends for K–S batteries.

can confine active materials (sulfur and corresponding sulfur-based species) and guarantee enough electrical contact;^[42] 2) dissolved K_2S_x polysulfides can be absorbed within the pores and further decrease the free migration of polysulfide intermediates to the anode;^[43] 3) volume fluctuations can be mitigated, ensuring the integrity of the sulfur cathode;^[44] and 4) electrolyte permeation is facilitated, promoting K ion transportation.^[14] The first article on the room-temperature K–S system reported the use of ordered mesoporous carbon (CMK-3)/sulfur and polyaniline (PANI)-coated CMK-3/sulfur composites as cathode materials, while the anode material was potassium metal. By conducting a melt-diffusion process, they impregnated different contents of S into the composites (**Figure 7a**). After galvanostatic tests, the composites without PANI and with loading of 40.8% S (**Figure 7c**) exhibited capacity of 512.7 mAh g^{-1} at current density of 50 mA g^{-1} . After 50 cycles at 50 mA g^{-1} , the composite achieved 202.3 mAh g^{-1} (**Figure 7b**). After protection by PANI, the performance of the composite was improved to 329.3 mAh g^{-1} after 50 cycles with the same current density (**Figure 7d**).^[16] Obviously, such performance is far from adequate for the practical application of the potassium–sulfur battery. The main challenges that have been posed have not been addressed. Thus, to achieve a better discharging/charging capacity, as well as, corresponding rate performance of the K–S system, more research work toward novel strategies should be

provided. In this section, we collect typical representative examples of the evolution of design principles for the sulfur cathode and divide them into three aspects, which are physical confinement, chemical attraction, and covalent binding.

4.1.1. Physical Confinement Strategy

Physical confinement is a physical method to build a specific structural skeleton to confine sulfur and suppress the migration of polysulfide intermediates, so that dissolution of polysulfides can be alleviated and sulfur loss reduced. With excellent conductivity, abundant porosity, and diverse structure, carbon-based materials not only provide enough surface area to trap polysulfide intermediates, but also act as electronic conductors to relieve the insulating properties of both electronic and protonic sulfur.^[45] With increasing temperature, the allotrope of S will change from ring-like S_8 to small sulfur molecules. When the temperature is higher than $600 \text{ }^\circ\text{C}$, S molecules undergo a high temperature and high pressure process, which decomposes them into S_2 .^[46] During this period, if an adequate carbon host exists with abundant microporous structure, the small sulfur molecules (S_2) will be trapped in the carbon matrix.^[47] At the same time, the micropore-enriched carbon matrix can confine the K_2S_y polysulfides and prevent

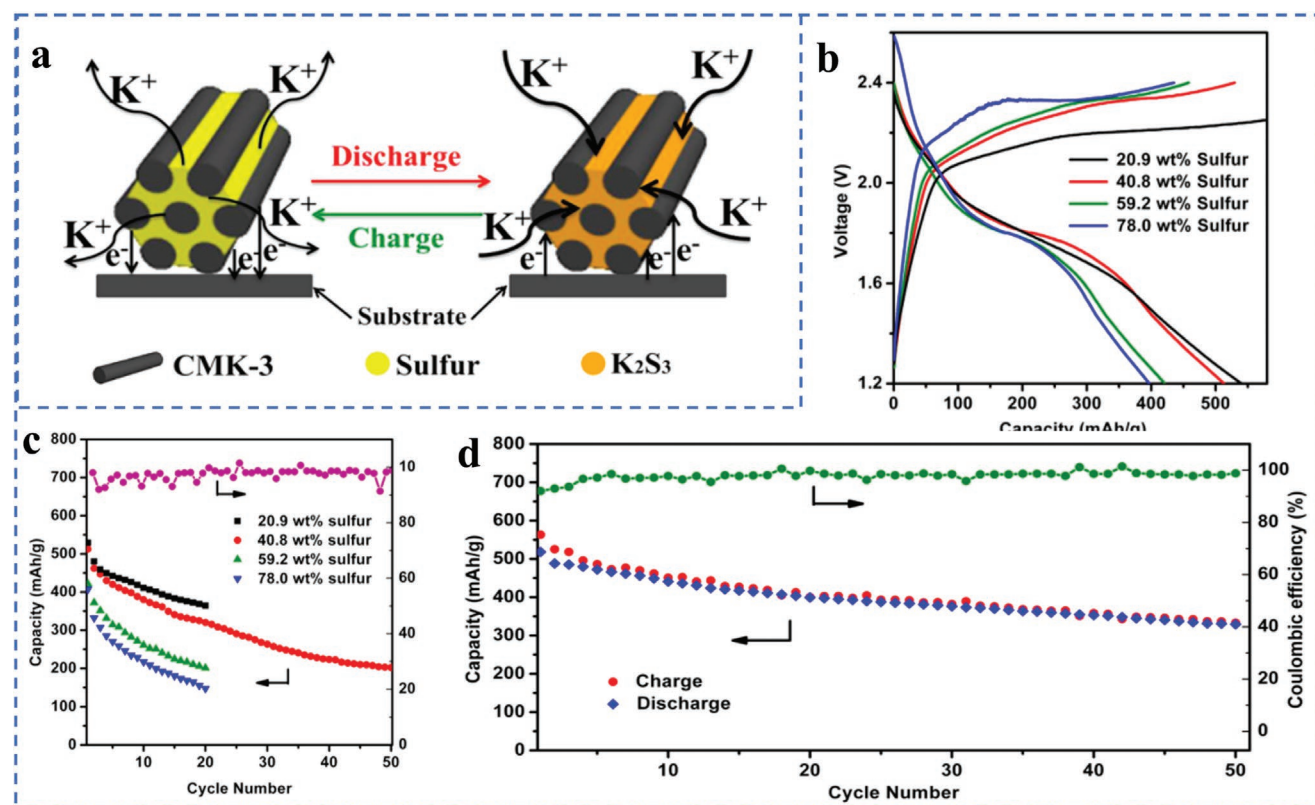


Figure 7. a) Schematic diagram of electrode reactions of rechargeable K–S batteries. b) Initial discharge and charge curves of K–S batteries using CMK-3/sulfur composites with different contents of S as the cathode at a current density of 50 mA g⁻¹. c) Cycling performance with different contents of S at 50 mA g⁻¹ and coulombic efficiency of selected 40.8 wt% S cathode. d) Cycling performance and coulombic efficiency at a current rate of 50 mA g⁻¹. Reproduced with permission.^[16] Copyright 2018, American Chemical Society.

them from forming soluble K₂S_x polysulfides. The most efficient method is to load the sulfur into a carbon host with abundant ultramicropores (diameter, $D \leq 0.5$ nm). Inspired by this, Xiong et al. synthesized microporous carbon by organic dehydration followed by high-temperature carbonization.^[25] After sulfur permeation at 600 °C, the microporous-carbon-loaded small sulfur species (C/S) were successfully obtained (Figure 8a). After using them as cathode materials, the C/S microporous composites delivered a high reversible capacity of 869.9 mAh g⁻¹ after 150 cycles with capacity loss of 0.18% every cycle at current density of 20 mA g⁻¹ (Figure 8b). As an advanced technology, TOF-SIMS was used for the first time to probe the carbon matrix, which was filled with micropores (Figure 8c). According to the analysis of the mass spectrum, the small sulfur allotropes are the main forms in which sulfur exists, which include single-atom sulfur, S₂, and S₃ (Figure 8d). Furthermore, medium- and K₂S_x sulfur molecules (S₄–S₇) are only adsorbed on the surface of the carbon host. In this case, the carbon host can block the formation of soluble K₂S_x polysulfides because of their strong confinement, which can further weaken the shuttle effect. The aim of the physical confinement strategy is mainly to minimize the dissolution of polysulfides and diffusion of sulfur species by means of interior physical adsorption and exterior physical blocking. In terms of physical confinement, development of an optimization strategy for the K–S system is still in its infancy. Even

though several researchers have carried out feasible studies to fabricate a range of C/S composites for sulfur cathode materials, the specific contribution of the pore-enriched materials is still unclear, which is because the K₂S₃ intermediate is always regarded as having the most thermodynamic stability among the polysulfides, making it hard to be further reduced.^[23,48] Furthermore, the sluggish reduction kinetics of insoluble K₂S₃ to K₂S₂ and K₂S also contribute to the incomplete reduction of sulfur. Hence, novel cathode materials with excellent conductivity and polysulfide affinity should be further explored. In addition, a flexible free-standing film, which was made of carbon nanotube and sulfur (CNT/S), was prepared to form a conductive network to function as a cathode for K–S batteries. Benefiting from the inter-crossing microchannels, the CNT/S film could provide rapid charge transfer and large active mass loading, which led to high initial capacity for the CNT/S film.^[49] Even so, it is unavoidable that a large amount of surface sulfur would cause side reactions, decreasing the active materials during discharging and charging processes. Therefore, removal of the superficial sulfur is an efficient approach to address this issue. Thus, by a facile filtration-washing method, Hu et al. fabricated non-superficial sulfur and deep impregnation sulfur. As a consequence, the obtained materials showed improved stability in their cycling performance.^[50] In addition, a series of sulfur-linked polymers, which contained various numbers of allyloxy linkers, were explored for their

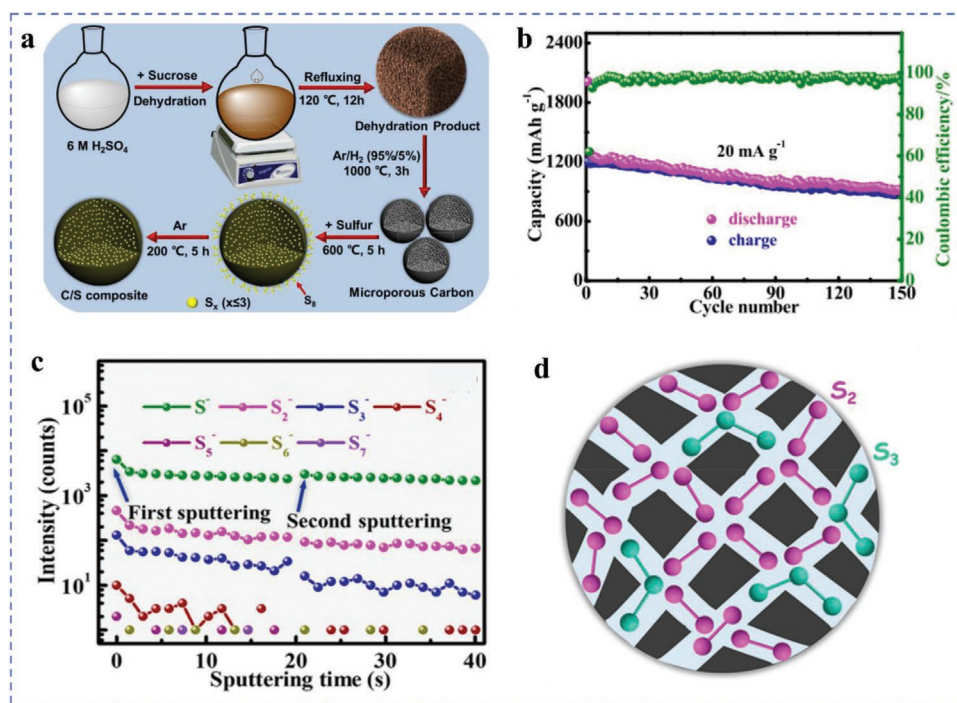


Figure 8. a) Schematic illustration of the formation of microporous C/S composite. b) Cycling performance and coulombic efficiency at 20 mA g⁻¹. c) TOF-SIMS data on the microporous C/S composite. d) Schematic illustration of the forms of sulfur existing in the porous carbon matrix: S₂ (purple) and S₃ (green). Reproduced with permission.^[25] Copyright 2019, American Chemical Society.

performance in K–S batteries. On testing the sulfur-linked tetra(allyloxy)-1,4-benzoquinone polymer (poly(S4-TABQ)) as a cathode material for K–S batteries, the active loading reached 71%, and it also delivered high capacity retention, 94.5% at 200 cycles (0.027% loss per cycle).^[51]

4.1.2. Chemical Interaction Strategy

Although the K–S system achieves decent results by virtue of physical confinement, most cathode materials usually exhibit non-polar bonds within non-polar surfaces, resulting in inferior interaction between the surface and the polysulfide intermediates. Consequently, the performance of 1-methylimidazole (Me-Im) solvated-copper achieved excellent reversible capacity of 922 mAh g⁻¹ at a high cell voltage of 1.93 V, which is equivalent to an unprecedented gravimetric power density of 1779 Wh (kg s)⁻¹. Such achievements were attributed to the copper (Cu) ion catalyst. After adding the Cu ions, the homogeneous Cu²⁺ ions could uniformly dissolve into the Me-Im electrolyte and accelerate catalysis of the transformation from S₃²⁻ to S²⁻. In particular, as illustrated in **Figure 9a**, compared with the potassium biphenyl anode (BpK)-S cell, the CV curve of BpK–S/Cu²⁺ shows a new redox peak at 2.5 V. This redox pair evidenced existence of the Cu²⁺/Cu⁺ couple, which is consistent with discharge capacity curves of BpK–S/Cu²⁺ at 2.5 V. In addition, the pure Cu cell exhibited a sharp decrease beginning at a 2.4 V after a voltage dip at 1.6 V and following a plateau at 1.4 V (Figure 9b). This phenomenon demonstrated that Cu⁺ underwent a reduction reaction to form Cu⁰, which was further characterized by

XRD measurements, as shown in Figure 9c. Compared with the pure S cell, the CV of the S/Cu²⁺ cell manifested two additional peaks, one reduction peak at 1.5 V and an oxidation peak at 1.7 V, respectively. These pairs were also absent for Cu²⁺. In this way, the results suggested that Cu²⁺ addition is beneficial for improving both discharge and charge capacities, which are due to the formation of S₂⁻ in the S/Cu²⁺ cell. This account was also verified by XPS (Figure 9d). In the XPS measurements of pure Cu²⁺, a strong reduction peak was located at 1.2 V, while it disappeared in the S/Cu²⁺ cell, which meant that the reduction of Cu⁺ to Cu⁰ did not happen in the S/Cu²⁺ cell. It is believed that the formation of insulating K₂S caused the absence of crystalline Cu metal. The final discharge products were also further measured by XRD. As shown in Figure 9b, the cathodes at different stages clearly exhibited various products during the discharging process. In the pure S cell, the crystalline phase of K₂S₃ was found after discharging finished (at the end of D3) (Figure 9c), while it was not observed in the S/Cu²⁺ cell. This feature demonstrated that Cu²⁺ played a crucial role in facilitating the further decomposition of K₂S₃. In terms of the pure Cu²⁺ cell, XRD showed that crystalline Cu metal existed after discharging, which was also identified from the assignment of Cu⁺/Cu at the voltage plateau <1.5 V. This result is consistent with CV and XPS, which indicated that the reduction of Cu⁺ to Cu⁰ would not occur in an S/Cu²⁺ cell. Overall, chemical interaction is a very promising and efficient strategy to weaken the S–S bonds and help to further catalyse the polysulfide intermediates, especially for K₂S₃, to obtain the final product K₂S. Such a strategy, however, is still in its early stages. More catalysts should be explored to enhance the performance of the

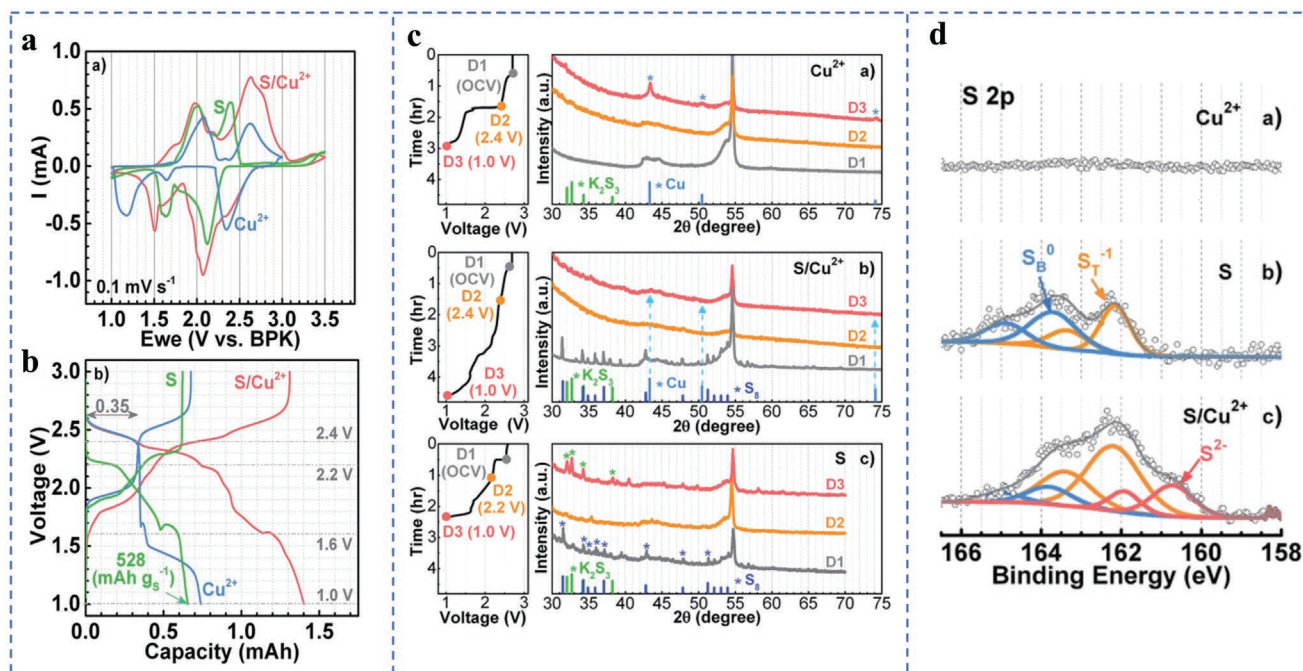


Figure 9. a) Cyclic voltammograms and b) first cycle galvanostatic voltage profiles of the BpK-S cell (green), the BpK-S/Cu²⁺ cell (red), and the BpK-Cu²⁺ cell (blue). c) The initial discharge curves (left) and XRD patterns of cathodes (right) from the BpK-Cu²⁺ cell (top), BpK-S/Cu²⁺ cell (middle), and BpK-S cell (bottom). d) S 2p XPS spectra of the fully discharged cathodes of the BpK-Cu²⁺ cell, BpK-S cell, and BpK-S/Cu²⁺ cell (from top to bottom). Reproduced with permission.^[34] Copyright 2017, Wiley-VCH.

K-S system. On the other hand, an advanced sulfur cathode can be designed by the combination of physical confinement and chemical interactions, which offers synergetic effects in achieving high-energy K-S batteries.

4.1.3. Covalent Fitting Strategy

Both physical confinement and chemical interaction can only minimize the dissolution of polysulfides but cannot address this issue fundamentally. To address this issue, the covalent fitting strategy helps to avoid this problem. Accordingly, Wu et al. fabricated a polyacrylonitrile (PAN)-sulfur polymer composite (SPAN) by a facile 450 °C annealing of a mixture of PAN and sulfur.^[23] After SPAN was applied as the cathode electrode material, it delivered the highest reversible capacity among all the sulfur cathodes. During the annealing process, sulfur played a role in facilitating the PAN cyclization process that occurs with the cleavage of nitrile groups and a following bonding with carbon in the neighboring groups (Figure 10a). According to the XRD, after PAN was fully carbonized to CPAN, a new peak emerged at 24.4°, and the peak for PAN moved from 17° to 15° (Figure 10b), which was consistent with graphitic (002) planes. As for SPAN, although there was a peak at 24.4°, the peaks of neither PAN nor S₈ existed on its XRD pattern. Also, from Figure 10c, the Raman spectra indicated that the intensity ratio of the G to the D band (I_G/I_D) of SPAN is stronger than that of CPAN, which suggested better crystallinity for SPAN, further demonstrating that PAN undergoes a better cyclization process with the assistance of sulfur, in accordance with the XRD results. Furthermore, the band at 460 cm⁻¹ could be attributed

to S-S stretching, while new peaks at 303 and 367 cm⁻¹ indicated C-S bonds. Fourier transform infrared (FTIR) spectra of CPAN and SPAN finally showed that C-S and S-S bonds both appeared in SPAN. Meanwhile, the bands at 1600, 1200, and 802 cm⁻¹ were all corresponding to π -conjugated hexacyclic rings with C=C and C=N bonds. The new peaks at 669 and 513 cm⁻¹ were attributed to C-S and S-S stretching modes. Combining the results of XRD, and Raman, and FTIR spectroscopy, it was concluded that the sulfur formed covalent bonds with the carbon in PAN in different forms during the cyclization process. With 0.8 m potassium hexafluorophosphate (KPF₆) in ethylene carbonate (EC):diethyl carbonate (DEC) = 1:1 (volume/volume (v/v)) as electrolyte, SPAN was evaluated for the K-S system and presented a high reversible capacity of 270 mAh g⁻¹ (710 mAh g⁻¹ based on sulfur mass) and excellent rate performance (Figure 10e,f). In addition, the PAN and sulfur were further developed by optimization at various temperatures and with various electrolytes. They assembled K-S batteries with 1 m potassium trifluoromethanesulfonate (KSO₃CF₃) in EC:DEC = 1:1 (v/v) as electrolyte. Apart from achieving excellent performance, it was very interesting that there was no shuttle effect due to the absence of redox processes of sulfur during potassiation and depotassiation. In addition, element doping is an efficient method to enhance the sulfur cathode capacitance and strengthen the interaction between K⁺ and the cathode. Overall, utilization of SPAN as cathode material in the K-S system always leads to excellent performance in both cycling and rate performance, which benefits from the covalent bonds between S = C, avoiding the shuttle effect and increasing the utilization rate of sulfur. Nevertheless, the previous reports related to PAN show that it cannot be used to prepare an electrode with

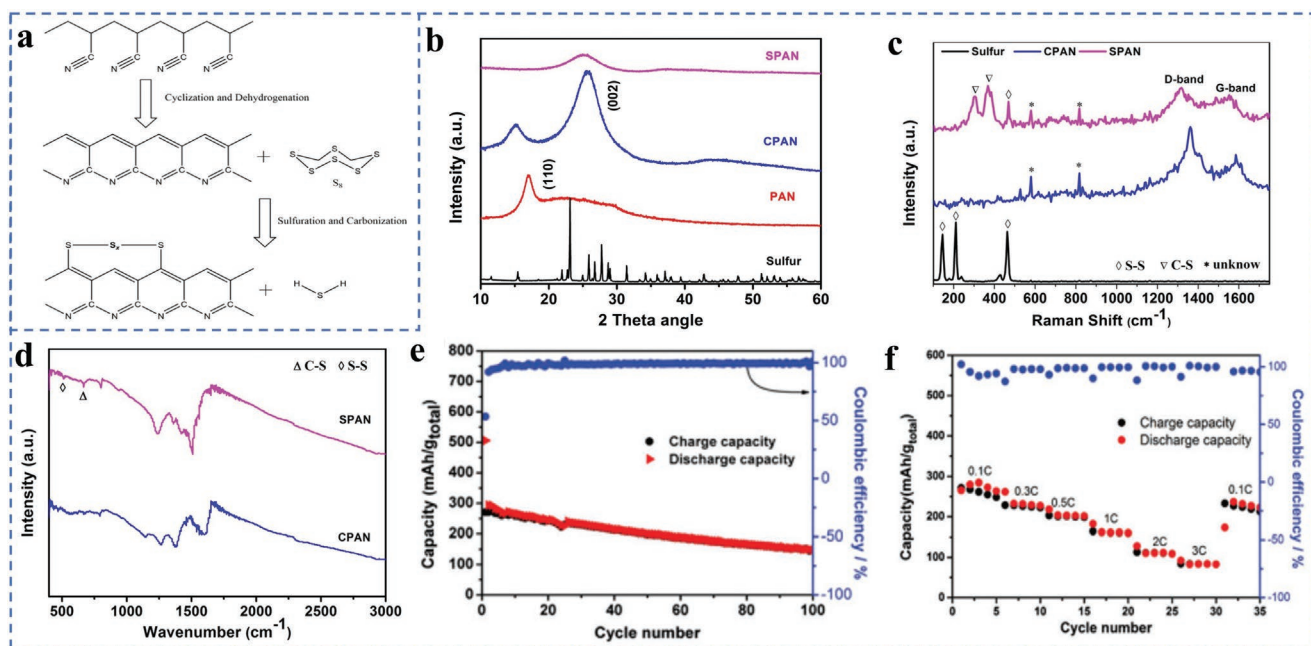


Figure 10. a) Schematic illustration of the synthesis process for SPAN. b) XRD patterns of SPAN, CPAN, PAN, and elemental sulfur. c) Raman spectra of SPAN, CPAN, and sulfur. d) FTIR spectra of SPAN and CPAN. e) Cycling stability and coulombic efficiency of SPAN at 0.5 C, and f) its rate capability from 0.1 to 3 C and corresponding coulombic efficiency. Reproduced with permission.^[23] Copyright 2018, Elsevier.

high sulfur loading. For instance, binders are always inactive materials, which cause lower gravimetric capacity and energy density. To solve this issue, a binder-free SPAN cathode was fabricated after a phase inversion and sulfurization process. The areal sulfur loading was up to 7 mg cm^{-2} , and the areal capacity was up to 4.2 mAh cm^{-2} . Such an improvement renders it a promising candidate for high energy density applications, which increases its applicability in large-scale fabrication.^[52]

4.1.4. Conductivity Improvement by Chalcogen Tailoring Strategy

Sulfur and its intermediates (K_2S_n , $n = 1-8$) have an insulating nature, which causes the low utilization ratio of sulfur.^[43a,53] Recently, many researchers found that using other chalcogens seems offer hope for resolving this unsettled issue.^[53b,54] Selenium (Se), which sits below sulfur in the periodic table, is widely used in the pigment and semiconductor industries. Compared with S, Se possesses stronger metallicity, since the larger atomic radius of Se causes weaker attraction of the outermost electrons. Se also has several advantages which the sulfur does not have: 1) The chain-structured allotrope h-Se is electroactive and easily stabilized due to its spatial confinement; and 2) if the Se is embedded in a porous host, it shows good compatibility with traditional and economical carbonate-based electrolytes. When they substituted Se for sulfur as the cathode active material, the above-mentioned issue for Li-S and Na-S batteries could be addressed, which were attributed to the higher electronic conductivity of Se ($1 \times 10^{-3} \text{ S m}^{-1}$ (Se) vs $5 \times 10^{-28} \text{ S m}^{-1}$ (Na)).^[55] 3) In addition to the higher electronic conductivity of Se, the K-Se batteries represent the advantage of the intermediate's phase change. Exactly, the Se

cathodes usually show the one-step Se redox reaction to converse to K_2Se . Benefiting from this advantage, the K-Se batteries can avoid the dissolution of long-chain intermediates, which prevents to formation shuttling effect.^[56] What's more, the lack of poly-selenides could prevent side reactions due to their low solubility in electrolytes.^[57] Therefore, K-Se batteries exhibit more stable electrochemical features, which express the high compatibility with electrolytes. Furthermore, studies indicated a higher energy density for Se_xS_y and better kinetic properties than either Se or S alone.^[58] Among the various Se_xS_y species, selenium disulfide (SeS_2) was the most prominent due to its better compatibility with carbonate-based electrolyte.^[59] A similar strategy can, of course, be applied to the K-S system. Hence, by coupling SeS_2 cathode and potassium anode, a K-Se S_2 battery could be created with a nitrogen-doped free-standing porous carbon fiber host (NCNFs) by means of electrospinning followed potassium hydroxides treatment, creating micropores.^[60] Then, the molten SeS_2 was transfused into the free-standing carbon host ($\text{SeS}_2@\text{NCNFs}$) (Figure 11a-c). When the self-supported $\text{SeS}_2@\text{NCNFs}$ was tested as cathode, it delivered a high reversible capacity, achieving 417 mA h g^{-1} over 1000 cycles at current density of 0.5 A g^{-1} (Figure 11d) and 703 mAh g^{-1} at current density of 0.05 A g^{-1} (Figure 11e), 100% coulombic efficiency, and 533 Wh kg^{-1} at 0.05 A g^{-1} (Figure 11f). The cyclic voltammograms (CVs) and voltage profiles clearly showed a two-step reaction with intermediate polysulfides and polyselenides. As can be observed in Figure 11g,h, the $\text{SeS}_2@\text{NCNFs}$ exhibited two cathodic peaks at 1.32 and 0.74 V during the potassiation process, which evidenced that the SeS_2 would react with K and be converted into K_2Se and K_2S . During the depotassiation process, there was only one peak located at 1.98 V, indicating that K_2Se and K_2S underwent a one-step

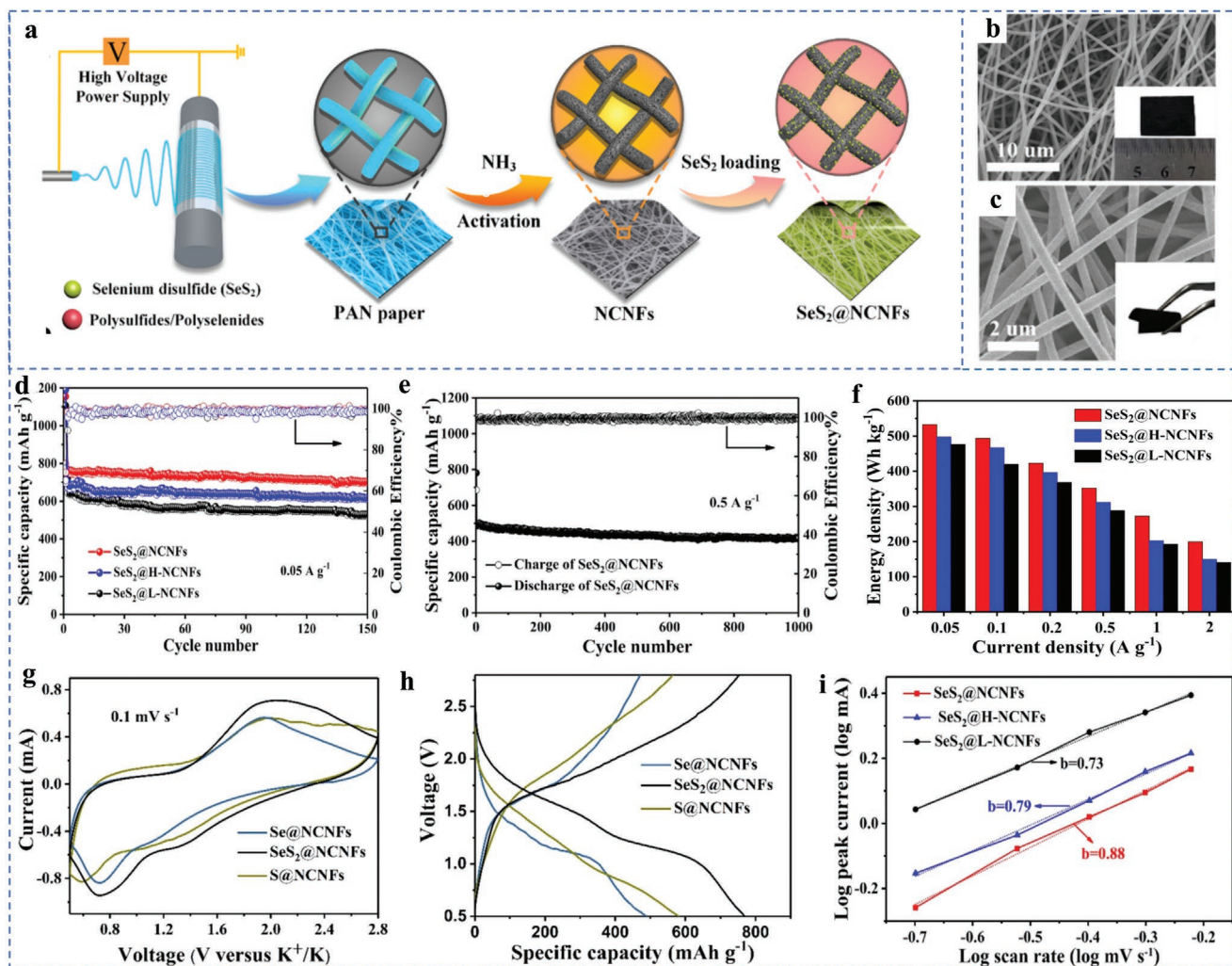


Figure 11. a) Synthesis procedure for the SeS_2 @NCNFs film electrode. b,c) SEM images of SeS_2 @NCNFs. The insets in (b) and (c) correspond to photographs of freestanding flexible SeS_2 @NCNFs films. d) Comparison of cycling performance at 0.05 A g^{-1} of SeS_2 @NCNFs, SeS_2 @H-NCNFs, and SeS_2 @L-NCNFs. e) Long-term cycling performance of SeS_2 @NCNFs at 0.5 A g^{-1} over 1000 cycles. f) Gravimetric energy density comparison of SeS_2 @NCNFs, SeS_2 @HNCNFs, and SeS_2 @L-NCNFs. Reproduced with permission.^[60] Copyright 2019, American Chemical Society.

conversion into SeS_2 . Compared with the CVs of Se@NCNFs and S@NCNFs , the redox peak profile of SeS_2 @NCNFs is similar but more symmetric, demonstrating that introducing Se into the S can improve the redox kinetics. In regards to the voltage profile of SeS_2 @NCNFs, two discharge plateaus and one charge plateau appeared separately in the discharging and charging processes, which corresponded with the CV curves, further confirming the two-step reaction and one-step reaction in the discharge and charge processes, respectively. What is more, the two-step and one-step reactions could avoid the formation of potassium polysulfides, which decreased the dissolution of polysulfides, enhancing the utilization ratio of active materials. Besides Se, tellurium (Te) is the last nonradioactive element in the chalcogen group, which endows it with the highest electrical conductivity of 2.5 S cm^{-1} among all of the non-metallic elements.^[61] Although Te exhibits the relatively inferior gravimetric specific capacity of 420 mAh g^{-1} due to the heavy atomic weight of Te, it provides an extremely high

volumetric specific capacity of 2621 mAh cm^{-3} , which is far beyond those of S and Se in the chalcogen group.^[62] Up to now, however, there has only been one report about Te for K energy storage.^[63] There is still much room for exploration based on the chalcogen tailoring strategy. The structural properties, fundamental physicochemical properties, and electrochemical theoretical knowledge of S, Se, and Te have been collected in Table 3 and Figure 12 for comparison. Even so, many concerns still exist. Se and Te are significantly rare elements in the Earth's crust with only 0.05 and 0.001 ppm crustal contents, respectively.^[64] The scarcity of selenium and tellurium imposes a very high price on their research.

To deal with the high cost and reserves issue for selenium, one method is using a combination of Se and S, which has been discussed above. The cost and reserves problem for tellurium still cannot be addressed at present. More efforts on the investigation of selenide- and telluride-based cathodes are required for further exploration. Therefore, tailoring the host

Table 3. Structures, fundamental physicochemical properties, and electrochemical theoretical knowledge of S, Se, Te.

Element and symbol	Sulfur (S)	Selenium (Se)	Tellurium (Te)
Electron configuration	[Ne]3s ² 3p ⁴	[Ar]3d ¹⁰ 4s ² 4p ⁴	[Kr]4d ¹⁰ 5s ² 5p ⁴
Electronegativity	2.58	2.55	2.10
Atomic mass	32.07	78.96	127.60
Atomic number	16	34	52
Atomic radius (pm)	88	103	123
Ionic radius (pm)	184 (-2), 29 (+6)	198 (-2), 42 (+6)	221 (-2), 56 (+6)
Melting point (°C)	115	221	450
Abundance in Earth's crust (ppm)	260	0.05	0.001
Electrical conductivity (S cm ⁻¹)	5 × 10 ⁻²⁸	1 × 10 ⁻³	2.5
Gravimetric specific capacity (mAh g ⁻¹)	1675	675	419
Volumetric specific capacity (mAh cm ⁻³)	3470	3253	2619
Price (data from Statista)	50 U.S. dollars per ton (in 2019)	≈23 759 U.S. dollars per ton (in 2017)	37 600 U.S. dollars per ton (in 2017)

with other materials that exhibit a stronger interaction than with physical confinement, would lead to better performance of sulfur cathode.

4.2. Strategies for Electrolytes

4.2.1. Novel Electrolytes

We first emphasize that priority should be granted to the development of electrolytes for the K–S system. The design of novel electrolytes is always of fundamental importance for the K–S battery, because the electrolyte sometimes determines the lower

limit and upper limit of these batteries. Novel electrolytes not only determine the stability and composition of the SEI layer, but also address the primal issue of the K–S system. Because K–S batteries share similarities with Li–S and Na–S batteries, many researchers have tried ester-based or ether-based electrolytes in the K–S system. Here, it should be noted that ester-based electrolytes are incompatible with sulfur and K₂S_x catholyte due to the nucleophilic feature of sulfur. The potassium salt KPF₆ is commonly employed in traditional carbonate solvents with a concentration of 0.8 M, which is due to the high ionic conductivity of K. Even so, the notorious shuttle issue has not been addressed, for example, by the use of TEGDME and diethylene glycol dimethyl ether (DEGDME). During the

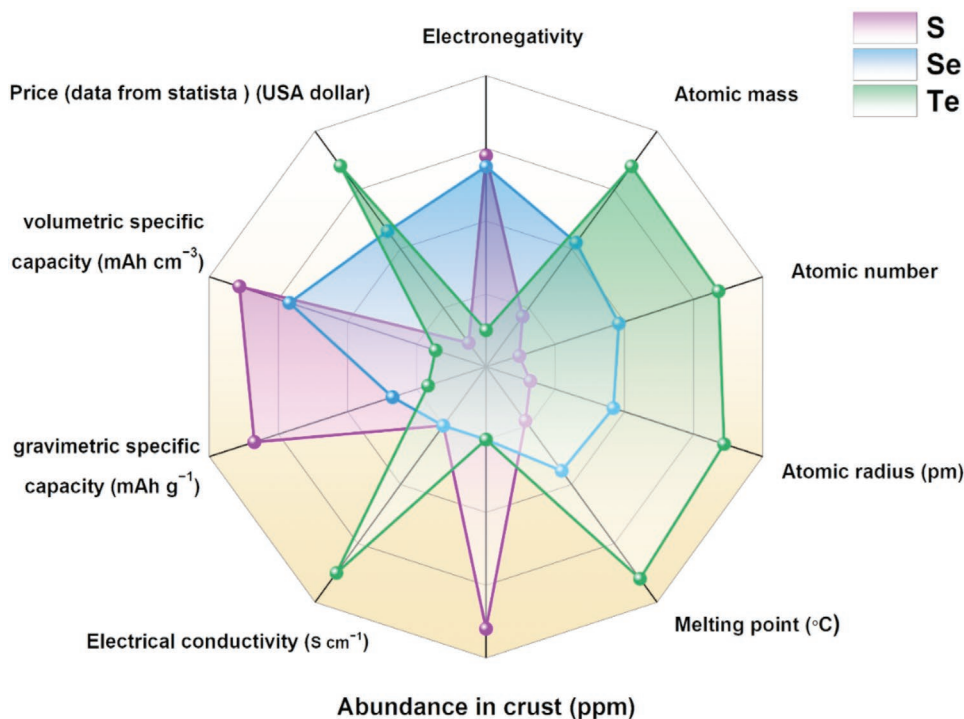


Figure 12. Comparison of physical properties for S, Se, and Te.

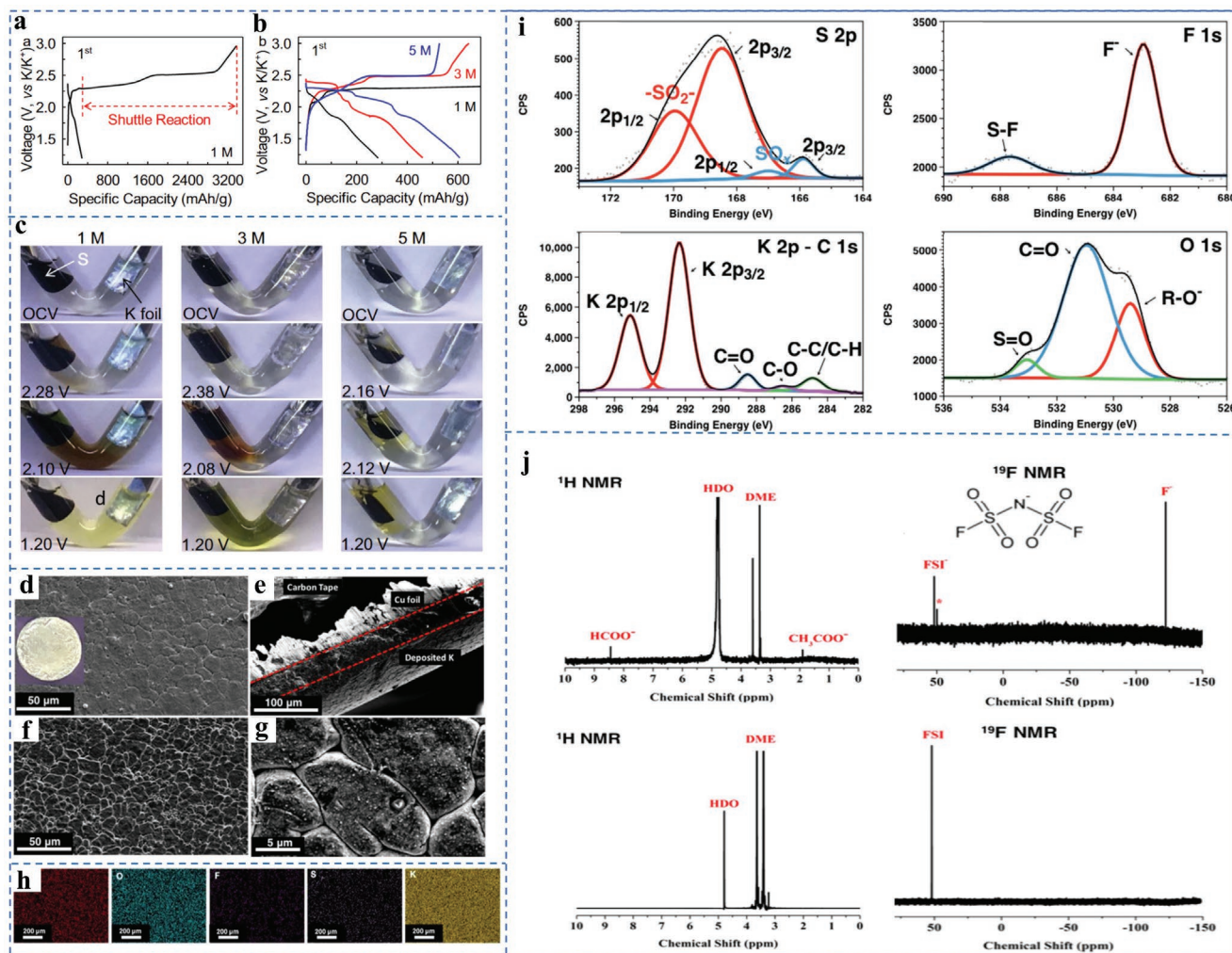


Figure 13. a,b) First-cycle voltage profiles of K–S batteries at 10 mA g^{-1} . c) “Transparent” batteries capture the polysulfides’ shuttle behavior. d) SEM imaging of K deposition at 0.05 mA cm^{-2} and e) the corresponding cross-sectional image. f) K deposition at 0.5 mA cm^{-2} and g) the zoomed-in image. h) The element distribution on the electrode surface. i) X-ray photoelectron spectroscopy (XPS) characterization of the K anode surface after cycling in KFSI/DME = 0.1 electrolyte. XPS spectra of the C 1s regions O 1s region, S 2p region, and F 1s region. j) The ^1H NMR and ^{19}F NMR spectra obtained from the K surface layer (top). The ^1H NMR and ^{19}F NMR spectra (bottom) of the electrolyte (extracted from the separator) after 200 cycles (over 1000 h). Reproduced with permission.^[32] Copyright 2019, Elsevier.

potassiation and depotassiation processes, the soluble polysulfide intermediates are mainly K_2S_6 and K_2S_4 , which can be considered as potassium salts. Their solubility has a particular degree of saturation for a given solvent. If a high concentration of a potassium salt exists in the solvent, it is bound to inhibit the further dissolution of other potassium salts. In addition, the high-concentration electrolyte must cause high viscosity, probably raising the pressure from the electrolyte to push back dendrite growth and achieve homogeneous deposition on the surface of the anode. The high viscosity also restrains anion convection near the deposition field, which is favorable for uniform deposition. Inspired by this, a concentrated electrolyte, which consisted of 5 m potassium trifluoromethanesulfonimide in DEGDM, was prepared and could effectively mitigate the shuttle effect.^[32] After employment in a K–S battery, it delivered $\approx 1270 \text{ Wh kg}^{-1}$ or $\approx 700 \text{ Wh kg}^{-1}$ at an average discharging voltage of 2.1 V. Three first-cycle profiles of K–S systems are

compared in Figure 13a,b. With increasing electrolyte concentration, higher reversible capacity was achieved. In the 5 m electrolyte, reversible capacity was high, around 527 mA h g^{-1} , with an initial CE of 86.96%, suggesting obvious depression of polysulfide dissolution and the shuttle effect. Subsequently, a visual experiment clearly showed the electrolyte concentration effect. As shown in Figure 13c, it was witnessed that brown colors in both 1 and 3 m electrolyte spread severely with the discharging reaction from $\approx 2.38 \text{ V}$ to $\approx 2.10 \text{ V}$ and at 1.20 V, while in 5 m electrolyte, the color on the anode side appeared to be light yellow, suggesting heavier dissolution as the concentration decreased. What is more, UV–vis absorption spectroscopy was further performed to verify the redox intermediates in 1, 3, and 5 m electrolytes. In the 5 m electrolyte, discharge products at 2.3, 2.1, and 1.2 V were dissolved in dimethyl ether (DME) and then detected by UV–vis absorption spectroscopy and ex situ XRD. It was concluded that both K_2S_6 and K_2S_5 coexist, and K_2S_n

($n = 4-6$) polysulfides were detected upon discharging to 2.3 and 2.1 V, respectively. As the discharging process continued toward 1.2 V, K_2S_3 was the only product observed. During the charging process, K_2S_4 was first found at 2.25 V. As the reaction proceeded, mixed K_2S_x ($x = 4, 5, 6$) was detected, and S_8 appeared at the final charging stage of 3 V. Apart from the suppression of polysulfide dissolution, novel electrolyte is recognized as a significant and crucial approach to inhibit dendrite growth for enhancement of the K-S system. Wu et al. fabricated a potassium bis(fluorosulfonyl)imide (KFSI)—dimethoxyethane (DME) electrolyte, which could promote a uniform SEI layer on the potassium anode, leading to very high efficiency ($\approx 99\%$) during potassium plating and stripping processes. The excellent reversibility of the potassium anode was attributed to the surface composition and morphology, so SEM, XPS, and NMR (1H and ^{19}F) were employed to analyse the K anode. From SEM observations, KFSI-DME would favor the formation of ordered surface morphology and compactness of the SEI layer (Figure 13d-g). Energy dispersive spectroscopy further revealed the elements composing the SEI layer, which consisted of C, O, F, S, and K elements (Figure 13h). After XPS (Figure 13i) and NMR (Figure 13j) were performed to probe the detailed chemical components of the K anode surface, they concluded that $-SO_2^-$, N-S, K-F, C-O, and C=O species were some crucial components of the SEI layer.

4.3. Electrolyte Additives

4.3.1. Solid State Electrolytes

Research on solid state electrolytes (SSEs) for K-S batteries is scanty. Borrowing experience from solid state potassium ion batteries and room-temperature (RT) Na-S batteries, the use of solid-state electrolytes is an effective way to solve safety issues and avoid polysulfides dissolution, thus improving the energy density. The SSEs can be divided into three classes, including solid polymer electrolytes (SPEs), inorganic solid electrolytes, and their combinations. Fei et al.^[65] employed an SPE electrolyte with 3,4,9,10-perylene-tetracarboxylic acid dianhydride (PTCDA) cathode in all-solid-state K ion batteries, which offered a high initial capacity of 118 mAh g^{-1} at 10 mA g^{-1} and a stable cycling performance. Feng's group further exploited inorganic based electrolytes, which is a new 3D open-framework potassium ferrite $K_2Fe_4O_7$, achieving a high voltage stability up to 5 V versus K/K⁺, for an all-solid-state potassium metal battery.^[66] By employing a Prussian blue cathode, the battery delivered a high charge/discharge rate of 250 C.

Although many materials exhibit high electrochemical performance in liquid electrolyte, they always show inferior irreversible capacity and non-ideal working voltages in solid-state electrolyte. This is due to the weak ionic mobility and unsatisfactory electronic conductivity, as well as, the inferior contact interphase with electrode materials for solid-state electrolytes. The insufficient contact interphase could impede both ions diffusion and electron charge transfer between different interphases, leading to the enhancement of resistance and polarization.

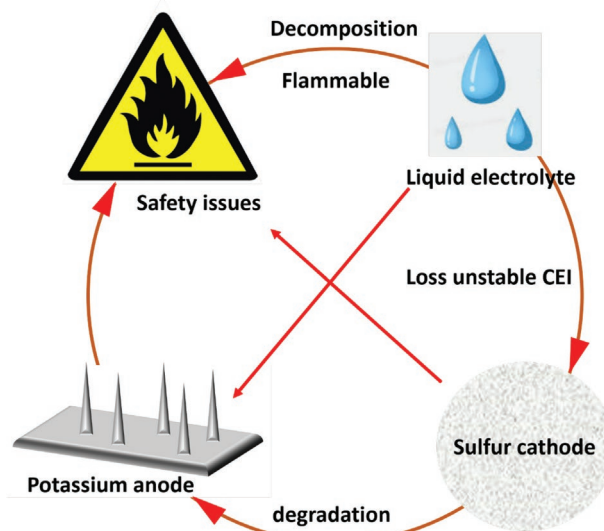


Figure 14. Summary of the aspects covered for K-S batteries.

4.4. Potassium Metal Anodes

4.4.1. Basic Understanding of Potassium Metal Instability

With a high specific capacity (687 mAh g^{-1}), the capacity of potassium metal is much higher than most anodes for potassium-ion batteries.^[67] It is very crucial to achieve a stable potassium plating and stripping. Otherwise, the unstable plating and stripping would cause inferior performance of any optimized S-based cathode (Figure 14). The plating and stripping of alkaline metals will cause large geometrical fluctuations, which take place between the growing/shrinking metal front and the spontaneous formed SEI film.^[68] Internal stresses in the potassium metal and significant stresses on the SEI will occur during the plating and stripping processes.^[69] Would the volume change be infinite when all the metal is stripped in every discharge of a K-S cell? When the anodic capacity is equal to the cathodic capacity, this assumption would hold. A too large or too thick anode would decrease the gravimetric capacity as well as the gravimetric energy. In the meantime, the more active potassium ions would be lost for a low cycling CE, which will reduce the life of the battery. When preparing K-S and K-K batteries in the laboratory, these batteries are always assembled with excessive K metal. Therefore, the volume changes caused by plating and stripping are always limited, while the low CE values are also weakened by this excess potassium metal. A 5% volume change in electrode height is caused when plating/stripping on the top 10 μm of a 200 μm thick potassium foil.^[11] Compared with the volume changes in sulfur cathode, the volume change on the anode side is very slight. With the development of K-S and K-K cells, thinner and more representative potassium metal anode should be further explored. Thus, the volume changes and low CE would be more severe. To date, there are many work focusing on lithium and sodium anodes, which can help us to realize the mechanism of plating and stripping, the function of electrolytes and electrode architectures in SEI formation, understanding, and dendrite growth control. At

present, work related to analogous analytical and modelling exploration of potassium anode has been rare. Basic knowledge of the potassium anode is still not clear. For instance, the mechanism that is adequate for mechanistic description of Li or Na metal growth is not suitable for K metal anode as well. This is because Li, Na, and K all have different features, such as in ion transport, mechanical strength, etc. Researchers have not assessed potassium dendrite growth with other conditions including plating current density and different electrolytes as well as additives. Therefore, it is obvious that our understanding of potassium metal anodes versus lithium or sodium anodes is different with respect to K–S versus Li–S or Na–S batteries. In addition, the stability of potassium anode mainly depends on its SEI. The SEI is formed from the reduction and decomposition of the electrolyte, which is because the Fermi energy of potassium is much larger than the lowest unoccupied molecular orbital in ester and ether electrolytes.^[70] The formation route for the SEI involves surface interphase chemistry, in which inorganic and organic compounds are generated on the surface of the potassium anode. The components are not fully established but include, for example, K_2CO_3 , potassium oxide (K_2O), potassium fluoride, $ROCO_2K$, etc.^[67d] As the SEI grows to a certain thickness, the SEI will be thick enough to prevent electrolyte decomposition.^[71] Some data in the research indicated that an unstable SEI on the potassium metal anode can continuously consume electrolytes, which is different from the SEI in Li and Na metal anodes. The resulting consequences would cause severe consumption of electrolyte and increased impedance. Hence, severe dendrite formation and even cell shorting would take place because of the unstable SEI.^[72] In contrast, a stable SEI can protect the potassium metal from corrosion and lead to uniform plating and stripping.

Generally speaking, dendrite growth is the crucial barrier to commercial Li–S batteries and is recognized as a main obstacle. The dendrite growth is generated by limited ion diffusion in the electrolyte and the establishment of localized electrical field concentration. Unlike Li and Na dendrite growth, the Sand's time is not suitable for K dendrite growth, since the morphology of the dendrites is mossy or forest-like instead of isolated. Meanwhile, the dendrite growth of K is usually focused on the places with intermediates or low current.^[73] An SEI always consists of multiple inorganic and organic phases that are intrinsically heterogeneous. These heterogeneities, including in physical, mechanical, and ion diffusion properties, in turn, contribute heterogeneous growth/dissolution of the potassium metal front, resulting in geometric instabilities, that is, dendrite growth. Compared with Li and Na, an unstable SEI would easily cause more severe dendrites, which is responsible for the K–S battery failure during the cycling. When a thick and non-uniform SEI exists, more heterogeneities will be produced and an enhanced electric field is unnecessary.^[68b,74] The potassium growth speed can be increased in some areas of the SEI, which are elastically softer, for instance, areas with pores and cracking. These areas accelerate K^+ ion diffusion and create priority nucleation sites including oxide and fluoride particles. This issue has not received any research or modelling. Therefore, it is very crucial to study the SEI structure and K ion diffusion as well as structural stability in the K–S battery. In terms of SEI on potassium metal anode, many variations in

internal interphase interfaces always exist. Researchers expect the diffusion speed of solid-state K ions on some internal interphase interfaces to be very fast, for instance, interphase interfaces containing K_2O – K_2CO_3 .^[75] According to the above, it is very necessary to study the SEI interphase interfaces and ion diffusion in the K–S battery. Studies on the SEI structure and ion transport in the K–S battery system are necessary. Supplementary simulation studies can be conducted to investigate the different inorganic SEI interfaces and surfaces. From research in the above articles, potassium dendrites grow more densely than lithium or sodium dendrites in analogous electrolytes. Potassium dendrites appear to be much more densely distributed than lithium dendrites in analogous liquid electrolytes. The mossy dendrite growth is an amplifying process, which causes the formation of a higher surface area and further increase greater SEI growth in subsequent cycling. There are obvious differences between potassium dendrites and lithium or sodium dendrites, including that the mossy potassium is more likely to grow on the root instead of on the tip (as for lithium or sodium dendrite growth). This is currently a hypothesis, which needs more detailed research to further confirm it.^[76] Wu and co-workers compared the CE of potassium metal anode in various electrolytes. As shown in **Figure 15a**, a uniform SEI formed on the surface of potassium in potassium bis(fluorosulfonyl)imide (KFSI)-dimethoxyethane (DME) electrolyte with a high efficiency $\approx 99\%$.^[67d] Then the galvanostatic discharge/charge curves and cycling performance (**Figure 15b,c**) were measured in a K/Cu cell, which indicated that a stable SEI quickly formed in the early stages of cell operation. In addition, the linear sweep voltammograms (**Figure 15d**) and Raman spectra (**Figure 15e**) exhibited improved oxidation durability for concentrated KFSI-DME electrolytes. As shown in **Figure 15f**, the feature of compatibility between KFSI/DME and potassium Prussian blue cathode was measured, which indicated that KFSI-DME electrolyte is an efficient and promising choice for the potassium anode. Apart from modified electrolyte, Goodenough et al. fabricated a K–Na liquid alloy for the potassium anode, serving as a dendrite-free anode (**Figure 15g–i**). Inspired by this work, many different Na–K alloy were continuously fabricated for potassium anode.^[77] Apart from K alloy, other strategies related to K anode are still very rare. To achieve better performance, more work should be carried out in the future.

4.5. Strategies for the Separator and Binder

Glass-fibre (Whatman) separator is usually assembled in test cells in K–S batteries. During the discharge and charge processes, the dissolved K_2S_x polysulfides easily pass through the separator and precipitate on the surface of the K anode. Actually, the glass fibre separators cannot efficiently prevent the shuttle effect of K_2S_x polysulfides. To endow separators with this function, the modified separators would need to trap polysulfides intermediates during cell operation, leading to enhanced specific capacity and cycling stability for K–S batteries. Inspired by functionalized separators for Li–S and Na–S batteries, the research effort on K–S batteries has also been efficient. Obvious shuttling suppression was reported by Manthiram et al. after a Celgard membrane was coated

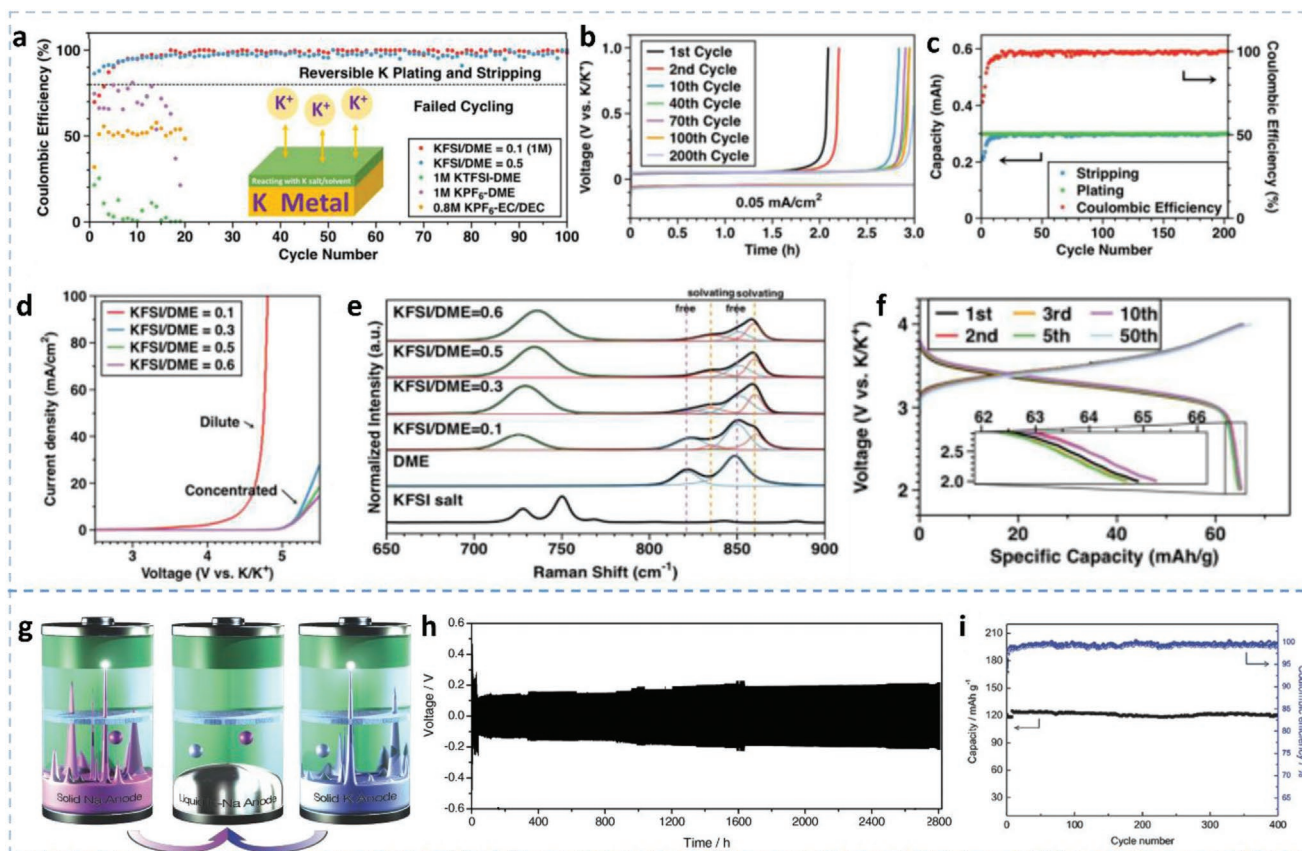


Figure 15. a) Comparing galvanostatic K plating and stripping on the Cu substrate among different electrolyte formulations at the rate of 0.05 mA cm^{-2} . b) Voltage profiles and c) cycling performance with KFSI-DME = 0.1 (1 m) electrolyte. d) Electrochemical stability of KFSI-DME electrolytes (Pt working electrode = 0.031 cm^2) and e) Raman spectra of KFSI-DME electrolytes with various concentrations (mole ratios). f) Voltage profiles of K/K/PB cell with KFSI-DME = 0.6 electrolyte (water < 15 ppm) at a rate of 100 mA g^{-1} (KPB). g) Schematic of making solid-metal anodes into liquid-alloy anode to suppress dendrite formation. Reproduced with permission.^[67d] Copyright 2019, American Chemical Society. h) Voltage versus time of a symmetric KNC-KNC cell cycled at 0.4 mA cm^{-2} with 2 h half cycles. i) Capacity and coulombic efficiency over 400 cycles at 1 C. Reproduced with permission.^[77] Copyright 2017, Wiley-VCH.

by single-wall carbon nanotubes to form as modified separator (Figure 16a).^[26] Such a modified separator could greatly immobilize polysulfides intermediates, causing an improved utilization rate of sulfur and enhanced cycling performance of K-S batteries (Figures 16b and 15c). To date, there have been few research efforts to improve the performance of K-S batteries by improving the separator. Performance optimization needs to be studied from a broad perspective. While the crucial function of a separator is to prevent short-circuits, superior separators are endowed with a range of additional advantages in the K-S battery system, such as suppressing the shuttling effect. With potassium anode, dendrites are a vital issue. In terms of conventional separators, a poor electrolyte wetting property and uneven pore size distribution would lead to an inhomogeneous ionic flux. Therefore, tailoring the separator is a novel and promising strategy to achieve long-term cycling of K-S batteries. Apart from the separator, the binder is also very important for K-S batteries. Unlike Li and Na, K would cause the larger volume changes during reduction/oxidation processes. Therefore, a binder with a better uniformity and stronger binding capability is very crucial to achieve an excellent performance in K-S batteries. To achieve

it, PAA was used as the binder for K-S batteries by Yang-Kook Sun et al. After PAA was used as the binder, the SPAN-based sulfur cathode demonstrated a great improvement when compared with PVDF as binder (Figure 16d,e).^[24] In addition, the cycled PAN based electrode expressed 10 times lower impedance than the SPAN electrode with PVDF binder, as shown in Figure 16f. In addition, many methods cannot be used to prepare electrodes with high sulfur loading and inactive binders have always reduced the gravimetric energy density. Thus, a binder-free SPAN cathode was fabricated by Lee et al. by conducting a phase inversion and sulfurization. The lack of binder caused a large enhancement for high-energy-density applications.

4.6. Comparisons of Energy Density and Cycling Performance among K-S Batteries

With the increasing demand for energy, in large-scale energy storage markets, K-S batteries will attract increasing attention due to their high energy density. In recent years, several developments have been achieved in K-S batteries. The comparisons

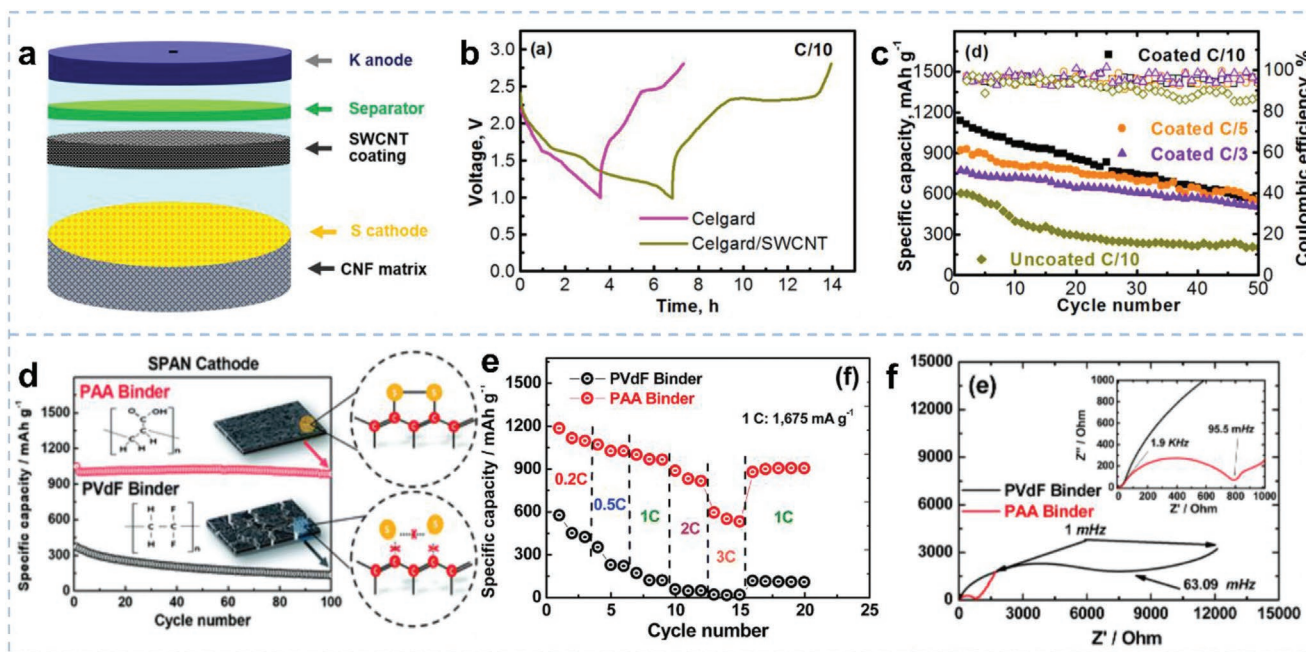


Figure 16. a) Schematic illustration of K–S cell (K||Celgard/SWCNT||S/CNF) with SWCNTs coating the Celgard separator on the cathode side. b) The effect of the SWCNT coating on the discharge/charge profiles. c) The effect of the coating on the cyclability of the cell. Reproduced with permission.^[26] Copyright 2018, Elsevier. Electrochemical performance of the SPAN electrode with poly(vinylidene difluoride) (PVDF) and PAA binders: d) cycle life test, e) rate capability test (sulfur loading amount in the SPAN electrode: 0.8 mg cm^{-2}), f) electrochemical impedance spectroscopy (EIS) measurements. Reproduced with permission.^[24] Copyright 2018, Wiley-VCH.

among the energy density of different reports are displayed in Figure 17a. The energy density depends on the average discharge voltage and specific capacity of the working cell. Benefiting from its large discharge capacity, PAA-binder-strengthened PAN electrode demonstrates an energy density of more than 1400 Wh kg^{-1} . As for poly(S4-TABQ) and CNT/S, although they have higher average voltage, lower capacities cause them to deliver lower energy densities. SPAN and confined and covalent sulfur (CCS) tend to show lower energy densities due to low accessible capacities and low average potentials. Overall, the energy density of K–S batteries exceeds those of Li-ion

batteries. In order to achieve high energy density, as discussed in Section 4, one effective way is to accelerate the kinetics of S redox reactions toward K_2S , thus delivering high reversible capacity. Another strategy is to realize elevated voltage plateaus via suppressing the shuttle effect and parasitic reactions. For instance, the utilization of highly concentrated electrolyte is capable of effectively hindering the shuttle effect of K_2S_x polysulfide intermediates under a widened charging threshold voltage of 3.0 V .^[32] The high reaction kinetics with a wide cut-off voltage is expected to unlock the full energy potential of K–S batteries.

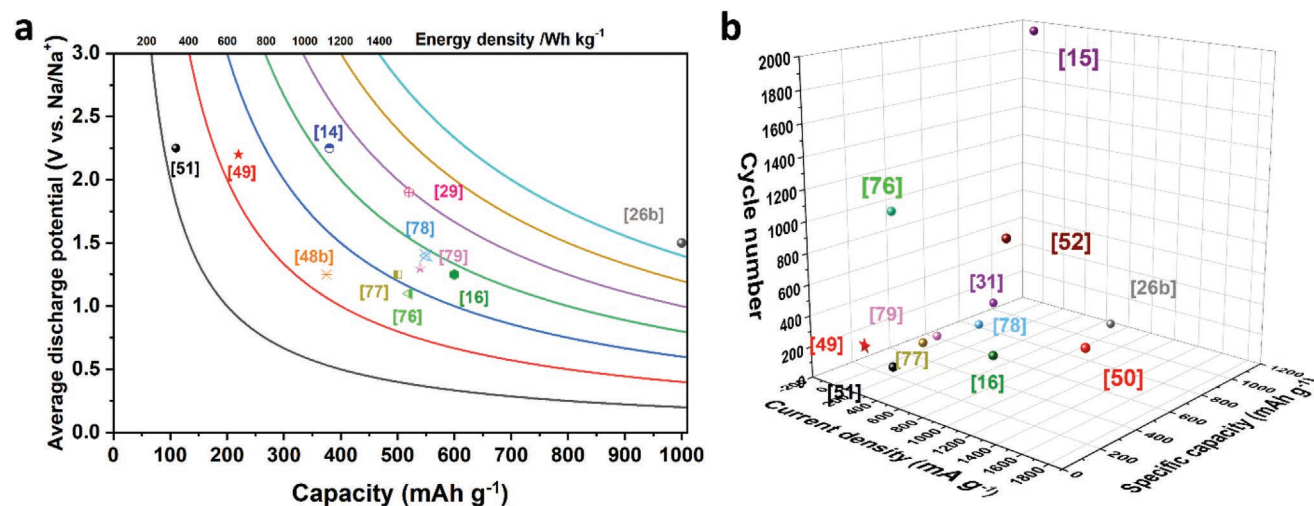


Figure 17. a) Comparison of the energy density of various K–S batteries. b) Comparison of the electrochemical performance of different K–S batteries.

Table 4. The cell components and electrochemical performances of representative K–S batteries.

Materials	Electrolyte	Current collector	Working current	Cycle number	Retained discharge capacity	Ref.
Covalent CCS	1 M KSO ₃ CF ₃ in EC/DEC	Al foil	150 mA g ⁻¹	300	253 mAh g ⁻¹	[78]
SPAN	0.8 M KPF ₆ in EC/DEC	–	0.5 C	100	147 mAh g ⁻¹	[23]
EAMC12 (C/S composites)	0.8 M KPF ₆ in EC/DEC	Al foil	0.2 C	500	281.2 mAh g ⁻¹	[50]
K–Na/SPAN	1 M KPF ₆ in EC/DMC/EMC	Al foil	35 mA g ⁻¹	100	140 mAh g ⁻¹	[79]
Poly(S ₄ -TABQ)	1 M KTFSI in TEGDME	Al foil	0.2 C	200	119 mAh g ⁻¹	[51]
SPAN electrode with PAA binder	0.5 M KPF ₆ in EC/DEC	Al foil	0.5 C	100	970 mAh g ⁻¹	[24]
CNT/S composite	3 M KFSI in DME	–	0.05 C	200	135 mAh g ⁻¹	[49]
I-S@pPAN	0.8 M in EC/DEC	Al foil	2 C	100	722 mAh g ⁻¹	[80]
S@SA-NC	0.8 M KPF ₆ in EC/DEC	Cu foil	0.5 C	200	371 mAh g ⁻¹	[20]
PCNF/S	0.8 M KPF ₆ in EC/DEC	–	20 mA g ⁻¹	2000	1002 mAh g ⁻¹	[19]
C/S composites	0.8 M KPF ₆ in EC/DEC	Al foil	20 mA g ⁻¹	150	869.9 mAh g ⁻¹	[25]
S–N–Co ₂ –C	0.8 M KPF ₆ in EC/DEC	Al foil	50 mA g ⁻¹	50	453 mAh g ⁻¹	[27]
FS-SPAN	1 M KFSI in EC/DEC	–	1 A g ⁻¹	1000	316 mAh g ⁻¹	[52]
Catholyte: Sulfur + K ₂ S _x	0.5 M KTFSI in DEGDME	–	0.1 C	20	310 mAh g ⁻¹	[14]
BpK–Cu ²⁺	1.0 M BpK in DME	–	0.48 C	200	540 mAh g ⁻¹	[34]

Furthermore, to highlight the performance of K–S batteries, the long cycling performance of all the K–S batteries is exhibited in Figure 17b and Table 4. The cycling stability of S cathodes is mainly determined by the reversibility of S redox reactions as well as the structural stability of S hosts. The porous carbon nanofibers/S electrode exhibited the best long cycling performance, achieving 2000 cycles with a capacity retention rate of 88%. This is ascribed to its microporous structure, which could enhance kinetics and suppress the dissolution of polysulfide intermediates, as well as achieving both strong physical and chemical confinement of S. It should be noted that high energy density and cycling performance were achieved with a very low current density, less than 0.5 C. High current results in large polarization, which further leads to the failure of potassium–sulfur batteries. Thus, more works and explorations should be focused on designing multifunctional S hosts. They are able to essentially achieve high electronic conductivity in the S cathode and ensure homogeneous S dispersion in the tailored hierarchical meso-/micro-porous structures. Moreover, introducing atomic catalysts into the tailored host architecture is expected to be an efficient tactic for high-performance K–S batteries, in terms of high reversible capacity, prolonged cycling stability, large energy density, and high rate capability.

5. Conclusion and Perspectives

In this review, we first discussed the mechanism of K–S batteries in detail. Next, all the scientific research works were summarized, including cathode materials, separators, electrolytes, and anodes. Although many tremendous improvements have been achieved in the past few years, there is still has long way to go before the K–S battery has been developed sufficiently for large-scale application. So far, reported work on the K–S battery system is far from excellent electrochemical performance.

Many challenges need to be further addressed, including the shuttling effect, sluggish reaction, severe side reactions, low ionic conductivity, dendrites, and electrolyte consumption, as well as, physical disintegration of electordes. More importantly, there is no K–S battery work related to full cells. Therefore, more research should be conducted in regard to cathode material design, electrolyte improvement, and anode optimization. It is highly desirable that means to suppress the shuttle effect and solve the safety hazard be found, which is the most important part for the commercialization process. Although these approaches seem too difficult for new progress, they are necessary to a certain degree. To achieve commercial application, we provide several perspectives on the K–S battery system: 1) A full understanding of the electrochemical reaction mechanism on the sulfur cathodes is the prerequisite for practical applications; 2) the cathodes should possess high conductivity, structural stability, and high sulfur loading, thus delivering high capacity and cycling life; 3) the raw materials and elements for the electrolytes should be non-toxic and cheap to avoid environmental and cost issues; and 4) stable interfaces are imperative, especially for the K anode/electrolyte interfaces. Here, several approaches are provided for K–S batteries (Figure 18). This may give assistance in paving the way to commercialization of K–S batteries.

5.1. Cathode Optimization

Unlike cathodes of Li–S and Na–S batteries, sulfur cathode in K–S batteries always exhibits low ideal capacity. It is because sulfur cathode always easily proceeds soluble long-chain polysulfide conversion reaction pathway from S₈ to K₂S₃ but difficultly conducts short-chain polysulfide conversion reaction pathway from K₂S₃ to K₂S. Thus, compared with Li–S and Na–S batteries, the K–S batteries usually deliver low ideal capacity and energy density. So far, the performance optimization of K–S

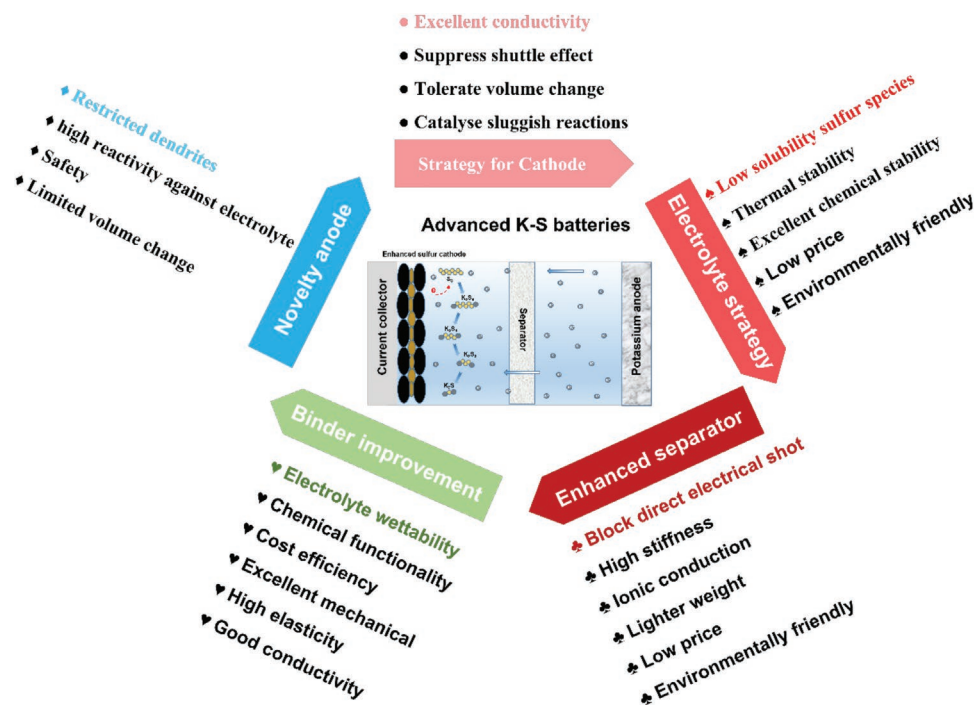


Figure 18. Perspectives and strategies on optimizing K–S batteries.

batteries is still lacking, significant effects of the proper hosts for high-capacity S cathode need to be further demonstrated. Cathodes with micropores and mesopores/micropores could be a promising direction for long-term stability of sulfur cathodes. Carbon materials with various morphologies and hierarchical nanostructures can serve as efficient hosts to embed S, for instance, carbon nanosheets, hollow carbon, porous carbon, etc. This method can be performed to improve the electronic conductivity of S cathodes and enable them to tolerate the huge volume changes during (de)potassiation processes. Apart from carbon materials, novel conductive materials should be investigated to embed sulfur while enhancing the tap density and reducing the proportion of inert materials. Furthermore, due to that sluggish kinetic reactions for solid–solid conversion pathways of K–S batteries, more polar electrocatalysts, including single atoms, metal oxides, metal sulfides, metal nitrides, and metal carbides, should be further explored, which can not only absorb polysulfides to suppress the shuttling effect, but also provide strong catalytic capacity to facilitate reversible solid–solid reactions, boosting the electrochemical performance of K–S batteries.^[81] The reported electrocatalysts can barely provide enough catalytic capability to redox reaction of sulfur. To build a highly active electrocatalyst with large surface area would be a promising approach for superior sulfur cathodes.

From the perspective of fundamental research, even though some achievements have been achieved by electrocatalysts, their classification is arbitrary. Evidence relating to the redox processes of polysulfide species should be further investigated. Therefore, more work should focus on the electrochemical mechanism on the cathode. To deeply explain the depotassiation and potassiation mechanisms is crucial to further improving the performance of the cathode, for instance, the redox reactions on the cathode during K–S cell operation

and the various types of electrochemical behavior of different electrolytes and electrocatalyst species. Furthermore, the redox reactions on the cathode related to dissociation and reconstruction of S–S bonds in polysulfide intermediates should be conducted and verified by experimental and theoretical calculation. More importantly, Advanced characterization techniques, such as synchrotron-based in situ and ex situ characterization techniques, should be employed and combined to investigate the electrochemistry. Advanced characterization techniques always can help us to deeply understand the electron transfer during charging and discharging processes.

For consideration of practical application, more efforts should be focused on investigating cathodes with high mass loading and high sulfur content in conjunction with lean electrolyte. In the meantime, more challenging methods need to design to achieve the scalable production of cathode materials, which can meet the needs of K–S battery applications, for example, spray-drying is a kind of approach that can be performed to meet the need for scalable production of cathode materials.

5.2. K Anode Improvement

The K anode itself is a crucial bottleneck problem for its commercialization. Compared with Li and Na anodes, the K anode is quite inadequate. To improve the K anode, several methods have been reported, which are similar to those for Li and Na anodes, including electrolyte modification by in situ SEI formation, 3D skeleton hosts, and alloying treatments, as well as artificial SEI layers. By manipulating the electrolytes, Na salts, and additives, SEI layers can be formed in situ on the surface of the K anode, which is a very simple way to protect the anode. In

addition, various artificial SEI layers with various compositions and structures represent an efficient approach to K stripping and plating. Nevertheless, the mechanical features, including flexibility and stiffness, should be improved for accommodating the structural changes of K and suppressing K dendrites. Moreover, it is easy to increase the interface impedance when artificial SEI layers are deposited on K metal anodes. Thus, to develop a thin SEI layer with proper mechanical features and high K-ion conductivity is a representative direction in the field of protection of K anodes.

5.3. Electrolyte Modification

The electrolyte is a very crucial component for the development of the overall electrochemical performance, and the surface interface chemistry of K–S batteries is also a representative conundrum for K–S batteries. The ideal electrolyte should be cost-efficient and be composed of environmental-friendly materials. At the same time, the electrolytes need to provide superior features, including high K-ion conductivity, a wide electrochemical stability window, no dendrite formation, no leakage, non-flammability, and good thermal stability.

So far, both ether-based and ester-based electrolytes are employed in the K–S battery, which enable the operation of K–S systems via different reaction pathways. However, there are still absent of ideal organic electrolytes that are able to effectively suppress parasitic reactions for both K anode and S cathode. The electrolyte and electrode can form the SEI and cathodic solid-state interphase (CEI) during the cell operation on the surfaces of both anode and cathode, respectively. Inspired by the effort in Li–S and Na–S batteries, one possible method to optimize electrolytes is adding additives. The additives can change the components of both anode and cathode, which further influence the performance of K–S batteries. Accordingly, a promising additive can efficiently suppress the decomposition of the electrolyte and inhibit the K metal dendrites. Fluoroethylene carbonate (FEC) is the most popular additive on both Li and Na metal anodes, which can stabilize the SEI layers of alkaline metal and improve the coulombic efficiency. Nevertheless, the FEC-based additive for K metal seem to be ineffective, which was ascribed to that the SEI is unstable after FEC decomposition on K anode.^[82] The liquid polysulfides, for instance, K_2S_8 , K_2S_6 , etc., could be also conducted as additives. This approach may enhance the charge transfer of solid potassium polysulfide intermediates, likes K_2S_3 , K_2S . On the other hand, the addition of soluble polysulfides compensate for the loss of active materials caused by side reaction on anode side. Additive-modified SEI is expected to protect the anode by suppressing the deposition of polysulfide intermediates while additive-modified CEI can protect the cathode so as to effectively prevent the dissolution of polysulfides. Besides, designation of a cathodic additive can decrease the activation voltage of insoluble polysulfide intermediates. Adding a redox mediator (RM) into the organic electrolyte is considered another efficient approach to enhance the performance of K–S batteries. By the aid of chemical oxidation of RMs in the electrolyte, such as organopolysulfide and quinone derivative in the electrolyte,^[83] the active materials (S) can be further chemically oxidized on the entire surface of RMs.

The additional charge transfer pathway would be different with the original electrocatalytic pathway, which promotes the homogeneous and complete oxidation reactions of the S cathode and thus decreases the overpotentials. Therefore, ideal RMs should accelerate the S redox reactions and exhibit strong redox regulation capability during the K–S battery operation.

Moreover, the solid-state electrolyte is also a promising direction because it can completely avoid the dissolution of polysulfides and dendrite growth. Furthermore, by using non-flammable solid-state electrolytes to replace flammable liquid electrolytes, the safety factor will be greatly enhanced. Therefore, it is a highly promising and large-scale energy storage application for the future. To better use solid electrolytes in the K–S battery, some fundamental features should be provided for guidance: 1) The solid electrolytes should be designed with high ionic conductivity, which increases the K ion diffusion and reduces the energy barrier; 2) the interphases, including cathode/electrolyte and anode/electrolyte interphases, are very crucial parts. This is because the capability of interfacial transport of K ions and electrons is the key prerequisite for all-solid-state batteries; 3) the solid electrolytes should have excellent contact with the electrodes to achieve a low interfacial resistance; and 4) the raw materials for solid electrolytes should be eco-friendly and cheap to meet environmental and cost issues.

5.4. Separator and Binder Enhancement

The separator does not actually take part in reactions during the cell operation. The structure and properties of the separator also cannot influence the energy density and powder density. Nevertheless, the separator should meet the required needs. First, chemical stability toward the electrode materials on both sides and electrolyte must be sufficient. Second, the mechanical properties should be improved, especially in liquid organic electrolytes. In these electrolytes, the separator can swell and thus introduce safety hazards. This swelling can affect the life of the battery since it can damage the cell if the separator is not mechanically strong. Third, the thermal properties of separators should be improved to match different working temperatures. Fourth, the separator should exhibit the excellent wettability so that it can be easily wetted by the electrolyte. It should also be porous, which facilitates the free flow of the electrolyte and ions while suppressing the flow of electrons.

The binder is always neglected for lithium and sodium storage. Due to the large size of potassium ions, however, the sulfur will suffer a large volumetric expansion, which is approximately 309% during the potassiation, when it is oxidized to potassium sulfides, rendering pulverization, structural damage, and even the physical disintegration of the electrode. To achieve excellent reversible cycling of the K–S battery, more advanced binder should be further designed to prepare electrode. To sum up, the novel binder should possess excellent mechanical stability and elastic properties, which can withstand large volume changes during the K–S battery operation. In addition, the superior binder can efficiently prevent electrolyte decomposition and the excellent swelling properties of the novel binder can efficiently help the electrolyte to permeate into the electrode materials instead of showing excessive penetration.

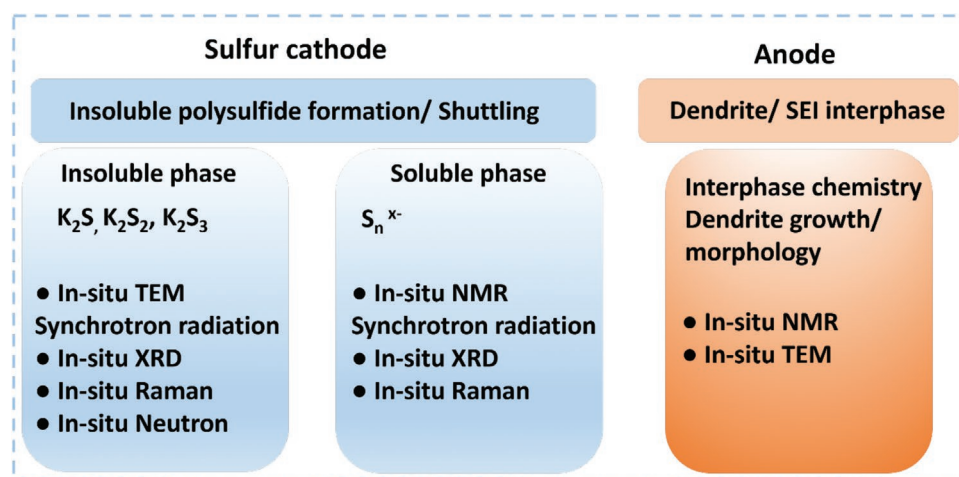


Figure 19. In situ characterization techniques for investigations on the K-S battery.

Furthermore, the binder should be light and conductive, resulting in enhancement of the electrochemical performance.

5.5. Advanced Characterization Methods

In situ characterization techniques have been commonly used to investigate the structural evolution of the electrode, active materials loss, and phase transformations, as well as polysulfides migration kinetics in the Li-S battery and Na-S battery.^[84] Nevertheless, it is significant to find that in situ characterization techniques are seldom used for K-S battery research. In situ based techniques are a very necessary range of techniques for acquiring a detailed understanding of physicochemistry of the K-S battery. With the assistance of in situ characterization techniques, we can fully recognize the issues and limitations of the K-S battery, which, in turn, improve the electrochemical performance. For instance, in situ XRD and in situ neutron diffraction (ND) require could detect the transformation of Bragg reflections from the crystallographic planes of K-S phase while in situ Raman spectroscopy and in situ NMR can achieve the transformation of chemical structural information on crystalline and amorphous phases.^[85] In situ TEM is a powerful tool yielding high-resolution spatial information on changes in morphology and structure. Small-angle neutron scattering and small-angle X-ray scattering can analyse the nano-to-microstructural bulk materials and observe the minute or microscopic regions.^[86] **Figure 19** lists the major challenges and corresponding in situ characterization techniques which could be conducted to explore these issues. The combination of advanced analytical instrumentation with in situ monitoring can provide a promising approach for addressing major technological challenges, then further provide deep insights to achieve a better understanding of the mechanisms in the K-S battery.

5.6. Perspective on Practical Application

Currently, both Li-S batteries and Na-S batteries are in a dominant position in both commercial and research fields. There

are several peculiar advantages that attract the researchers to pursue the possibility of K-S batteries. Unlike polysulfide intermediates of Li-S and Na-S batteries, a series of K_2S_n ($1 \leq n \leq 6$) intermediates can be stable at room temperature. Thus, a series of potassium polysulfide catholytes can be prepared, which could act as a source for active liquid S intermediates and as a K ions conducting medium. By using the catholyte as the cathode, the upper cut-off potential have to be controlled to suppress the shuttling effect. For instance, the cut-off voltage is changed to below 2.4 V. On the anode side, the constructed K-S cell can utilize cheap graphite rather than expensive hard carbon as its anode, which avoids the safety concerns coming from the employment of potassium metal on the anode side. Although the current electrochemical performance of K-S batteries is generally poor, advances in research have revealed the great potential of K-S batteries in the future. These advantages in terms of high safety and low cost further highlight the feasibility the practical applications of K-S batteries. As a novel battery technology, many challenges accompany great opportunities, which researchers need to explore. Therefore, there will be a long road to achieve practical applications of K-S batteries for large-sale stationary energy storage.

Acknowledgements

Y.-J.L., H.-L.Y., and Y.L. contributed equally to this work. This research was supported by the Australian Research Council (ARC) (DE170100928, DE220101113, DP200100365) and an Australian Renewable Energy Agency (ARENA) Project (G00849). The authors also thank Dr. Tania Silver for her critical reading of the manuscript.

Open access publishing facilitated by University of Wollongong, as part of the Wiley - University of Wollongong agreement via the Council of Australian University Librarians.

Conflict of Interest

The authors declare no conflict of interest.

Keywords

energy storage systems, K–S batteries, optimization strategies, polysulfides, potassium anodes, sulfur cathodes

Received: July 24, 2022

Revised: September 10, 2022

Published online: October 30, 2022

- [1] a) X. Yang, J. Luo, X. Sun, *Chem. Soc. Rev.* **2020**, *49*, 2140; b) J. Liu, *Adv. Funct. Mater.* **2013**, *23*, 924.
- [2] a) D. R. Deng, F. Xue, C.-D. Bai, J. Lei, R. Yuan, M. S. Zheng, Q. F. Dong, *ACS Nano* **2018**, *12*, 11120; b) K. Kubota, M. Dahbi, T. Hosaka, S. Kumakura, S. Komaba, *Chem. Rec.* **2018**, *18*, 459; c) Y.-J. Lei, Z.-C. Yan, W.-H. Lai, S.-L. Chou, Y.-X. Wang, H.-K. Liu, S.-X. Dou, *Electrochem. Energy Rev.* **2020**, *3*, 766.
- [3] X. Zhao, Y. Lu, Z. Qian, R. Wang, Z. Guo, *EcoMat* **2020**, *2*, e12038.
- [4] V. Anoopkumar, B. John, T. D. Mercy, *ACS Appl. Energy Mater.* **2020**, *3*, 9478.
- [5] Y.-J. Wang, B. Fang, D. Zhang, A. Li, D. P. Wilkinson, A. Ignaszak, L. Zhang, J. Zhang, *Electrochem. Energy Rev.* **2018**, *1*, 1.
- [6] B. Li, J. Zhao, Z. Zhang, C. Zhao, P. Sun, P. Bai, J. Yang, Z. Zhou, Y. Xu, *Adv. Funct. Mater.* **2019**, *29*, 1807137.
- [7] a) K. W. Guji, W.-C. Chien, F.-M. Wang, A. Ramar, E. B. Chemere, L. Tiong, L. Merinda, *Nanomaterials* **2021**, *11*, 3120; b) P. Münster, A. Heckmann, R. Nölle, M. Winter, K. Beltrop, T. Placke, *Batteries Supercaps* **2019**, *2*, 992.
- [8] S. Komaba, T. Hasegawa, M. Dahbi, K. Kubota, *Electrochem. Commun.* **2015**, *60*, 172.
- [9] a) C. Senthil, S.-S. Kim, H. Y. Jung, *Nat. Commun.* **2022**, *13*, 145; b) H. Liu, W.-H. Lai, Y. Lei, H. Yang, N. Wang, S. Chou, H. K. Liu, S. X. Dou, Y.-X. Wang, *Adv. Energy Mater.* **2022**, *12*, 2103304.
- [10] a) R. Fang, S. Zhao, Z. Sun, D.-W. Wang, H.-M. Cheng, F. Li, *Adv. Mater.* **2017**, *29*, 1606823; b) N. Chawla, M. Safa, *Electronics* **2019**, *8*, 1201.
- [11] J. Ding, H. Zhang, W. Fan, C. Zhong, W. Hu, D. Mitlin, *Adv. Mater.* **2020**, *32*, 1908007.
- [12] X. Yuan, B. Zhu, J. Feng, C. Wang, X. Cai, R. Qin, *J. Power Sources* **2020**, *480*, 228874.
- [13] L. Ni, M. Osenberg, H. Liu, A. Hilger, L. Chen, D. Zhou, K. Dong, T. Arlt, X. Yao, X. Wang, Y. Chen, Y. Li, K. Zhao, C. Yang, I. Manke, F. Sun, R. Chen, *Nano Energy* **2021**, *83*, 105841.
- [14] J.-Y. Hwang, H. M. Kim, C. S. Yoon, Y.-K. Sun, *ACS Energy Lett.* **2018**, *3*, 540.
- [15] N. Cheng, P. Xu, B. Lu, Z. Liu, *J. Energy Chem.* **2021**, *62*, 645.
- [16] Q. Zhao, Y. Hu, K. Zhang, J. Chen, *Inorg. Chem.* **2014**, *53*, 9000.
- [17] X. Lu, M. E. Bowden, V. L. Sprenkle, J. Liu, *Adv. Mater.* **2015**, *27*, 5915.
- [18] Y. Liu, Z. Tai, Q. Zhang, H. Wang, W. K. Pang, H. K. Liu, K. Konstantinov, Z. Guo, *Nano Energy* **2017**, *35*, 36.
- [19] X. Zhao, Y. Hong, M. Cheng, S. Wang, L. Zheng, J. Wang, Y. Xu, *J. Mater. Chem. A* **2020**, *8*, 10875.
- [20] C. Ye, J. Shan, D. Chao, P. Liang, Y. Jiao, J. Hao, Q. Gu, K. Davey, H. Wang, S.-Z. Qiao, *J. Am. Chem. Soc.* **2021**, *143*, 16902.
- [21] J. Shao, J. Zheng, L. Qin, S. Zhang, Y. Ren, Y. Wu, *Angew. Chem., Int. Ed.* **2022**, *61*, e202200606.
- [22] X. Yuan, B. Zhu, J. Feng, C. Wang, X. Cai, K. Qiao, R. Qin, *Small* **2020**, *16*, 2003386.
- [23] Y. Liu, W. Wang, J. Wang, Y. Zhang, Y. Zhu, Y. Chen, L. Fu, Y. Wu, *Chem. Commun.* **2018**, *54*, 2288.
- [24] J.-Y. Hwang, H. M. Kim, Y.-K. Sun, *J. Mater. Chem. A* **2018**, *6*, 14587.
- [25] P. Xiong, X. Han, X. Zhao, P. Bai, Y. Liu, J. Sun, Y. Xu, *ACS Nano* **2019**, *13*, 2536.
- [26] X. Yu, A. Manthiram, *Energy Storage Mater.* **2018**, *15*, 368.
- [27] X. Ge, H. Di, P. Wang, X. Miao, P. Zhang, H. Wang, J. Ma, L. Yin, *ACS Nano* **2020**, *14*, 16022.
- [28] A. Manthiram, Y. Fu, Y.-S. Su, *Acc. Chem. Res.* **2013**, *46*, 1125.
- [29] F. Yang, S. M. A. Mousavie, T. K. Oh, T. Yang, Y. Lu, C. Farley, R. J. Bodnar, L. Niu, R. Qiao, Z. Li, *Adv. Energy Mater.* **2018**, *8*, 1701991.
- [30] a) J. C. Wheeler, *J. Chem. Phys.* **1984**, *81*, 3635; b) R. F. Bacon, R. Fanelli, *J. Am. Chem. Soc.* **1943**, *65*, 639; c) X. Ji, K. T. Lee, L. F. Nazar, *Nat. Mater.* **2009**, *8*, 500; d) W. J. Chung, J. J. Griebel, E. T. Kim, H. Yoon, A. G. Simmonds, H. J. Ji, P. T. Dirlam, R. S. Glass, J. J. Wie, N. A. Nguyen, B. W. Guralnick, J. Park, Á. Somogyi, P. Theato, M. E. Mackay, Y.-E. Sung, K. Char, J. Pyun, *Nat. Chem.* **2013**, *5*, 518; e) J. Zhu, P. Zhu, C. Yan, X. Dong, X. Zhang, *Prog. Polym. Sci.* **2019**, *90*, 118; f) R. Fang, J. Xu, D.-W. Wang, *Energy Environ. Sci.* **2020**, *13*, 432.
- [31] X. Tang, D. Zhou, P. Li, X. Guo, B. Sun, H. Liu, K. Yan, Y. Gogotsi, G. Wang, *Adv. Mater.* **2020**, *32*, 1906739.
- [32] L. Wang, J. Bao, Q. Liu, C.-F. Sun, *Energy Storage Mater.* **2019**, *18*, 470.
- [33] S. Gu, N. Xiao, F. Wu, Y. Bai, C. Wu, Y. Wu, *ACS Energy Lett.* **2018**, *3*, 2858.
- [34] N.-C. Lai, G. Cong, Y.-C. Lu, *J. Mater. Chem. A* **2019**, *7*, 20584.
- [35] a) D. K. Lee, S. J. Kim, Y.-J. Kim, H. Choi, D. W. Kim, H.-J. Jeon, C. W. Ahn, J. W. Lee, H.-T. Jung, *Adv. Mater. Interfaces* **2019**, *6*, 1801992; b) Y. Lei, C. Wu, X. Lu, W. Hua, S. Li, Y. Liang, H. Liu, W.-H. Lai, Q. Gu, X. Cai, N. Wang, Y.-X. Wang, S.-L. Chou, H.-K. Liu, G. Wang, S.-X. Dou, *Angew. Chem., Int. Ed.* **2022**, *61*, e202200384; c) C. Wu, Y. Lei, L. Simonelli, D. Tonti, A. Black, X. Lu, W.-H. Lai, X. Cai, Y.-X. Wang, Q. Gu, S.-L. Chou, H.-K. Liu, G. Wang, S.-X. Dou, *Adv. Mater.* **2022**, *34*, 2108363.
- [36] S. Lee, J. Lee, J. Kim, M. Agostini, S. Xiong, A. Matic, J.-Y. Hwang, *Energies* **2020**, *13*, 2791.
- [37] a) J. Lei, T. Liu, J. Chen, M. Zheng, Q. Zhang, B. Mao, Q. Dong, *Chem* **2020**, *6*, 2533; b) C. Wu, Y. Lei, L. Simonelli, D. Tonti, A. Black, X. Lu, W.-H. Lai, X. Cai, Y.-X. Wang, Q. Gu, S.-L. Chou, H.-K. Liu, G. Wang, S.-X. Dou, *Adv. Mater.* **2021**, *34*, 2108363; c) J. H. Lee, J. Kang, S.-W. Kim, W. Halim, M. W. Frey, Y. L. Joo, *ACS Omega* **2018**, *3*, 16465.
- [38] a) S.-S. Fan, H.-P. Liu, Q. Liu, C.-S. Ma, T.-F. Yi, *J. Materiomics* **2020**, *6*, 431; b) H. Huang, J. Wang, X. Yang, R. Hu, J. Liu, L. Zhang, M. Zhu, *Angew. Chem., Int. Ed.* **2020**, *59*, 14504.
- [39] S. Wang, Y. Yan, D. Xiong, G. Li, Y. Wang, F. Chen, S. Chen, B. Tian, Y. Shi, *Angew. Chem., Int. Ed.* **2021**, *60*, 25122.
- [40] H. Sun, P. Liang, G. Zhu, W. H. Hung, Y.-Y. Li, H.-C. Tai, C.-L. Huang, J. Li, Y. Meng, M. Angell, C.-A. Wang, H. Dai, *Proc. Natl. Acad. Sci. U. S. A.* **2020**, *117*, 27847.
- [41] a) J. Zhu, J. Zou, H. Cheng, Y. Gu, Z. Lu, *Green Energy Environ.* **2019**, *4*, 345; b) C. Wu, W.-H. Lai, X. Cai, S.-L. Chou, H.-K. Liu, Y.-X. Wang, S.-X. Dou, *Small* **2021**, *17*, 2006504.
- [42] a) L. Borchardt, M. Oschatz, S. Kaskel, *Chemistry* **2016**, *22*, 7324; b) S. Li, T. Mou, G. Ren, J. Warzywoda, B. Wang, Z. Fan, *ACS Energy Lett.* **2016**, *1*, 481; c) H.-J. Peng, J.-Q. Huang, Q. Zhang, *Chem. Soc. Rev.* **2017**, *46*, 5237.
- [43] a) X. Zhao, Y. Lu, Z. Qian, R. Wang, Z. Guo, *EcoMat* **2020**, *2*, e12038; b) E. P. Kamphaus, P. B. Balbuena, *J. Phys. Chem. C* **2016**, *120*, 4296.
- [44] T. Yang, Y. Niu, Q. Liu, M. Xu, *Nano Mater. Sci.* **2022**.
- [45] a) T. Ali, C. Yan, *ChemSusChem* **2020**, *13*, 1447; b) M. Wu, J. Liao, L. Yu, R. Lv, P. Li, W. Sun, R. Tan, X. Duan, L. Zhang, F. Li, J. Kim, K. H. Shin, H. S. Park, W. Zhang, Z. Guo, H. Wang, Y. Tang, G. Gorgolis, C. Galiotis, J. Ma, *Chem Asian J* **2020**, *15*, 995.
- [46] a) Y. Wang, Y. Zhang, H. Cheng, Z. Ni, Y. Wang, G. Xia, X. Li, X. Zeng, *Molecules* **2021**, *26*, 1535; b) X. Zhao, G. Cheruvally, C. Kim,

- K.-K. Cho, H.-J. Ahn, K.-W. Kim, J.-H. Ahn, *J. Electrochem. Sci. Technol.* **2016**, 7, 97.
- [47] K. Zhu, C. Wang, Z. Chi, F. Ke, Y. Yang, A. Wang, W. Wang, L. Miao, *Front. Energy Res.* **2019**, 7, 123.
- [48] S. Wei, L. Ma, K. E. Hendrickson, Z. Tu, L. A. Archer, *J. Am. Chem. Soc.* **2015**, 137, 12143.
- [49] X. Yuan, B. Zhu, J. Feng, C. Wang, X. Cai, R. Qin, *J. Electron. Mater.* **2021**, 50, 3037.
- [50] L. Hu, X. Meng, L. Liu, D. Liang, S. Liang, L.-L. Wang, L. Yang, T. Ding, C. Deng, Q. Dong, *Chem. Commun.* **2021**, 57, 1490.
- [51] L. Zhang, L. Ge, G. He, Z. Tian, J. Huang, J. Wang, D. J. L. Brett, J. Hofkens, F. Lai, T. Liu, *J. Phys. Chem. C* **2021**, 125, 18604.
- [52] K. Yang, S. Kim, X. Yang, M. Cho, Y. Lee, *Small Methods* **2022**, 6, 2100899.
- [53] a) Y. Li, H. Zhan, S. Liu, K. Huang, Y. Zhou, *J. Power Sources* **2010**, 195, 2945; b) Y. Fu, Z. Wu, Y. Yuan, P. Chen, L. Yu, L. Yuan, Q. Han, Y. Lan, W. Bai, E. Kan, C. Huang, X. Ouyang, X. Wang, J. Zhu, J. Lu, *Nat. Commun.* **2020**, 11, 845; c) C. Weller, J. Pampel, S. Dörfler, H. Althues, S. Kaskel, *Energy Technol.* **2019**, 7, 1900625.
- [54] a) A. Eftekhari, *Sustainable Energy Fuels* **2017**, 1, 14; b) R. Kumar, J. Liu, J.-Y. Hwang, Y.-K. Sun, *J. Mater. Chem. A* **2018**, 6, 11582.
- [55] a) H. Tian, H. Tian, S. Wang, S. Chen, F. Zhang, L. Song, H. Liu, J. Liu, G. Wang, *Nat. Commun.* **2020**, 11, 5025; b) F. Li, Z. Wei, A. Manthiram, Y. Feng, J. Ma, L. Mai, *J. Mater. Chem. A* **2019**, 7, 9406; c) L. Wang, X. Zhang, L. Deng, J. Tang, H. Deng, W. Hu, Z. Liu, *ACS Appl. Mater. Interfaces* **2019**, 11, 4995.
- [56] a) X. Huang, J. Sun, L. Wang, X. Tong, S. X. Dou, Z. M. Wang, *Small* **2021**, 17, 2004369; b) X. L. Huang, Z. Guo, S. X. Dou, Z. M. Wang, *Adv. Funct. Mater.* **2021**, 31, 2102326; c) X. Huang, J. Deng, Y. Qi, D. Liu, Y. Wu, W. Gao, W. Zhong, F. Zhang, S. Bao, M. Xu, *Inorg. Chem. Front.* **2020**, 7, 1182.
- [57] a) X. Huang, Q. Xu, W. Gao, T. Yang, R. Zhan, J. Deng, B. Guo, M. Tao, H. Liu, M. Xu, *J. Colloid Interface Sci.* **2019**, 539, 326; b) X. Huang, W. Wang, J. Deng, W. Gao, D. Liu, Q. Ma, M. Xu, *Inorg. Chem. Front.* **2019**, 6, 2118.
- [58] a) H. Du, S. Feng, W. Luo, L. Zhou, L. Mai, *J. Mater. Sci. Technol.* **2020**, 55, 1; b) S. Zhang, D. Yang, H. Tan, Y. Feng, X. Rui, Y. Yu, *Mater. Today* **2020**, 39, 9; c) Q.-T. Xu, H.-G. Xue, S.-P. Guo, *Inorg. Chem. Front.* **2019**, 6, 1326.
- [59] a) Z. Li, J. Zhang, Y. Lu, X. W. Lou, *Sci. Adv.* **2018**, 4, eaat1687; b) Z. Li, J. Zhang, H. B. Wu, X. W. Lou, *Adv. Energy Mater.* **2017**, 7, 1700281.
- [60] Y. Yao, R. Xu, M. Chen, X. Cheng, S. Zeng, D. Li, X. Zhou, X. Wu, Y. Yu, *ACS Nano* **2019**, 13, 4695.
- [61] a) N. Nitta, F. Wu, J. T. Lee, G. Yushin, *Mater. Today* **2015**, 18, 252; b) J. B. Goodenough, Y. Kim, *Chem. Mater.* **2010**, 22, 587; c) J. W. Choi, D. Aurbach, *Nat. Rev. Mater.* **2016**, 1, 16013.
- [62] F. Wu, J. Maier, Y. Yu, *Chem. Soc. Rev.* **2020**, 49, 1569.
- [63] S. Dong, D. Yu, J. Yang, L. Jiang, J. Wang, L. Cheng, Y. Zhou, H. Yue, H. Wang, L. Guo, *Adv. Mater.* **2020**, 32, 1908027.
- [64] a) W. Zhang, Y. Liu, Z. Guo, *Sci. Adv.* **2019**, 5, eaav7412; b) R. Borah, F. R. Hughson, J. Johnston, T. Nann, *Mater. Today Adv.* **2020**, 6, 100046.
- [65] H. Fei, Y. Liu, Y. An, X. Xu, G. Zeng, Y. Tian, L. Ci, B. Xi, S. Xiong, J. Feng, *J. Power Sources* **2018**, 399, 294.
- [66] H. Yuan, H. Li, T. Zhang, G. Li, T. He, F. Du, S. Feng, *J. Mater. Chem. A* **2018**, 6, 8413.
- [67] a) B. Cao, Q. Zhang, H. Liu, B. Xu, S. Zhang, T. Zhou, J. Mao, W. K. Pang, Z. Guo, A. Li, J. Zhou, X. Chen, H. Song, *Adv. Energy Mater.* **2018**, 8, 1801149; b) Q. Zhang, Z. Wang, S. Zhang, T. Zhou, J. Mao, Z. Guo, *Electrochem. Energy Rev.* **2018**, 1, 625; c) Q. Zhang, C. Didier, W. K. Pang, Y. Liu, Z. Wang, S. Li, V. K. Peterson, J. Mao, Z. Guo, *Adv. Energy Mater.* **2019**, 9, 1900568; d) N. Xiao, W. D. McCulloch, Y. Wu, *J. Am. Chem. Soc.* **2017**, 139, 9475.
- [68] a) W. Cao, X. Yu, H. Li, *eScience* **2022**, 2, 47; b) W. Liu, P. Liu, D. Mitlin, *Adv. Energy Mater.* **2020**, 10, 2002297.
- [69] a) J. H. Cho, X. Xiao, K. Guo, Y. Liu, H. Gao, B. W. Sheldon, *Energy Storage Mater.* **2020**, 24, 281; b) B. Horstmann, J. Shi, R. Amine, M. Werres, X. He, H. Jia, F. Hausen, I. Kecik-Laskovic, S. Wiemers-Meyer, J. Lopez, D. Galvez-Aranda, F. Baakes, D. Bresser, C.-C. Su, Y. Xu, W. Xu, P. Jakes, R.-A. Eichel, E. Figgemeier, U. Krewer, J. M. Seminario, P. B. Balbuena, C. Wang, S. Passerini, Y. Shao-Horn, M. Winter, K. Amine, R. Kostecki, A. Latz, *Energy Environ. Sci.* **2021**, 14, 5289.
- [70] L. Li, S. Zhao, Z. Hu, S.-L. Chou, J. Chen, *Chem. Sci.* **2021**, 12, 2345.
- [71] a) K. Ushirogata, K. Sodeyama, Z. Futera, Y. Tateyama, Y. Okuno, *J. Electrochem. Soc.* **2015**, 162, A2670; b) J. Tan, J. Matz, P. Dong, J. Shen, M. Ye, *Adv. Energy Mater.* **2021**, 11, 2100046.
- [72] B. Wu, J. Lochala, T. Taverne, J. Xiao, *Nano Energy* **2017**, 40, 34.
- [73] a) Y. Yan, C. Shu, R. Zheng, M. Li, Z. Ran, M. He, A. Hu, T. Zeng, H. Xu, Y. Zeng, *Nano Res.* **2021**, 15, 3150; b) P. Bai, J. Li, F. R. Brushett, M. Z. Bazant, *Energy Environ. Sci.* **2016**, 9, 3221; c) G. Yoon, S. Moon, C. Ceder, K. Kang, *Chem. Mater.* **2018**, 30, 6769.
- [74] K. W. Guji, W.-C. Chien, F.-M. Wang, A. Ramar, E. B. Chemere, L. Tiong, L. Merinda, *Nanomaterials* **2021**, 11, 3120.
- [75] a) J. Popovic, *J. Electrochem. Soc.* **2022**, 169, 030510; b) P. Liu, D. Mitlin, *Acc. Chem. Res.* **2020**, 53, 1161.
- [76] W. Mu, X. Liu, Z. Wen, L. Liu, *J. Energy Storage* **2019**, 26, 100921.
- [77] a) L. Xue, H. Gao, Y. Li, J. B. Goodenough, *J. Am. Chem. Soc.* **2018**, 140, 3292; b) L. Zhang, X. Xia, Y. Zhong, D. Xie, S. Liu, X. Wang, J. Tu, *Adv. Mater.* **2018**, 30, 1804011; c) D. Tang, T. Wang, W. Zhang, Z. Zhao, L. Zhang, Z.-A. Qiao, *Angew. Chem., Int. Ed.* **2022**, 61, e202203967.
- [78] R. Ma, L. Fan, J. Wang, B. Lu, *Electrochim. Acta* **2019**, 293, 191.
- [79] Y. Zhang, J. Lou, Y. Shuai, K. Chen, X. He, Y. Wang, N. Li, Z. Zhang, F. Gan, *Mater. Lett.* **2019**, 242, 5.
- [80] S. Ma, P. Zuo, H. Zhang, Z. Yu, C. Cui, M. He, G. Yin, *Chem. Commun.* **2019**, 55, 5267.
- [81] a) X. L. Huang, S. X. Dou, Z. M. Wang, *Mater. Horiz.* **2021**, 8, 2870; b) X. L. Huang, S. X. Dou, Z. M. Wang, *Energy Storage Mater.* **2022**, 45, 265; c) X. L. Huang, Y.-X. Wang, S.-L. Chou, S. X. Dou, Z. M. Wang, *Energy Environ. Sci.* **2021**, 14, 3757.
- [82] T. Hosaka, S. Muratsubaki, K. Kubota, H. Onuma, S. Komaba, *J. Phys. Chem. Lett.* **2019**, 10, 3296.
- [83] a) Y. Tsao, M. Lee, E. C. Miller, G. Gao, J. Park, S. Chen, T. Katsumata, H. Tran, L.-W. Wang, M. F. Toney, Y. Cui, Z. Bao, *Joule* **2019**, 3, 872; b) M. Zhao, B.-Q. Li, X. Chen, J. Xie, H. Yuan, J.-Q. Huang, *Chem* **2020**, 6, 3297.
- [84] a) J. Tan, D. Liu, X. Xu, L. Mai, *Nanoscale* **2017**, 9, 19001; b) M. Li, Z. Amirzadeh, R. De Marco, X. F. Tan, A. Whittaker, X. Huang, R. Wepf, R. Knibbe, *Small Methods* **2018**, 2, 1800133; c) F. Jin, B. Wang, J. Wang, Y. Wang, Y. Ning, J. Yang, Z. Zhang, P. Liu, Y. Zhou, D. Wang, H. Liu, S. Dou, *Matter* **2021**, 4, 1768; d) L. Wang, T. Wang, L. Peng, Y. Wang, M. Zhang, J. Zhou, M. Chen, J. Cao, H. Fei, X. Duan, J. Zhu, X. Duan, *Natl. Sci. Rev.* **2022**, 9, nwab050.
- [85] a) H.-L. Wu, L. A. Huff, A. A. Gewirth, *ACS Appl. Mater. Interfaces* **2015**, 7, 1709; b) H. Wang, N. Sa, M. He, X. Liang, L. F. Nazar, M. Balasubramanian, K. G. Gallagher, B. Key, *J. Phys. Chem. C* **2017**, 121, 6011.
- [86] S. Risse, E. Härk, B. Kent, M. Ballauff, *ACS Nano* **2019**, 13, 10233.



Yao-Jie Lei received his Bachelor's degree at Lanzhou University and his Master's degree from the University of Manchester and the University of Sydney. He is currently a Ph.D. student at the Institute for Superconducting and Electronic Materials (ISEM), University of Wollongong (UOW) under the supervision of Dr. Yun-Xiao Wang and Prof. Shi Xue Dou. His research is focused on electrocatalysts, sodium-ion batteries, sodium–sulfur batteries, and potassium–sulfur batteries.



Wei-Hong Lai is a Research Fellow at the Institute for Superconducting and Electronic Materials (ISEM), University of Wollongong (UOW). He received his Bachelor's degree (2011) from Hebei United University and his Master's degree (2014) from Beijing University of Technology. He obtained his Ph.D. degree from the University of Wollongong in 2019. His current research interest is renewable energy storage and conversion, including electrocatalysis, the lithium–air battery, and sodium–sulfur batteries.



Yun-Xiao Wang is a Senior Research Fellow at the Institute for Superconducting and Electronic Materials (ISEM), University of Wollongong (UOW). She received her Master's degree (2011) from Xiamen University and obtained her Ph.D. degree from the University of Wollongong in 2015. Her current research interest is renewable energy storage and conversion, including electrocatalysis, lithium/sodium-ion batteries, and lithium/sodium metal batteries.